

Tadeja Saje, Matjaž Vidmar

Abstract

Thanks to the many independent technological achievements in the recent years, serious radio astronomy is again within reach of amateur astronomers. Observation of the $\lambda=21\text{cm}$ neutral-hydrogen line is relatively straightforward, since the strongest hydrogen clouds in our galaxy achieve an equivalent back-body brightness temperature of around $T \approx 100\text{K}$. Yet such observation provides important information about the structure and velocity of our galaxy. In this article the design, construction and calibration of a suitable radio telescope is discussed in detail making efficient use of available hardware and software. Important practical details like radio-interference mitigation in an urban environment are also discussed. Finally, the results obtained with the prototype radio telescope are presented both as the hydrogen spectra in selected directions as well as a 3D map (galactic longitude, galactic latitude and velocity profile) of our Milky Way galaxy visible from our latitude 46° north.

Povzetek

Številni med sabo neodvisni tehnološki dosežki zadnjih nekaj let omogočajo, da je resna radioastronomija ponovno dostopna amaterskim astronomom. Opazovanje spektralne črte atomarnega vodika $\lambda=21\text{cm}$ je razmeroma preprosto, saj spektralna svetlost najmočnejših oblakov vodika v naši galaksiji dosega enakovredno temperaturo sevanja črnega telesa okoli $T \approx 100\text{K}$. Hkrati takšno opazovanje daje pomembne informacije o sestavi in hitrosti naše galaksije. V tem prispevku so podrobno opisani načrtovanje, izgradnja in umerjanje primerenega radioteleskopa ob učinkoviti uporabi razpoložljive strojne in programske opreme. Opisane so tudi pomembne praktične podrobnosti, kot je izogibanje radijskim motnjam v mestnem okolju. Končno, rezultati meritev z izdelanim prototipom radioteleskopa so prikazani kot spektri atomarnega vodika v izbranih smereh in kot 3D zemljevid (galaktična dolžina, galaktična širina in profil hitrosti) naše galaksije Rimske ceste, kot jo vidimo iz naše zemljepisne širine 46° severno.

1. Amateur radio astronomy

For many thousand years, astronomy was limited to optical observations in the visible part of the electromagnetic spectrum. Finally, in middle of the 20th century the first successful observations of celestial radio and microwave sources were made. Today astronomical observations are made over all of the electromagnetic spectrum. Space-based telescopes may be required at wavelengths where the Earth's atmosphere is opaque to electromagnetic waves.

Visible-light observations remain the most popular even today. Large and extremely expensive professional instruments are located at carefully-selected remote sites with clear skies and low levels of light pollution. Besides these large professional instruments, amateur optical observations with much smaller instruments located at non-perfect sites still play an important role in the science of astronomy. For example, most new asteroids are discovered by amateur observers.

Although the very first radio map of the sky was plotted by an amateur astronomer, Grote Reber in 1938-1946 [1], radio astronomy quickly evolved into using extremely large antennas and sophisticated signal processing, all of them out of reach of amateurs. On the other side, it is worth noting that the most important discoveries of early radio astronomy like the non-thermal radiation of many celestial sources including the Sun, the $\lambda=21\text{cm}$ neutral-hydrogen line or the cosmic

background radiation were made with relatively simple equipment originally designed for a completely different purpose.

Things started changing in favor of amateur radio astronomy after about 1990. The widespread deployment of satellite television made medium-size parabolic antennas and corresponding positioners available to amateurs. The semiconductor industry mastered III-V semiconductors, in particular GaAs based HEMTs allowing exceptionally low-noise receivers operating at room temperature well into the microwave region. Both allowed successful amateur observations of the $\lambda=21\text{cm}$ neutral-hydrogen line [2].

At the turn of the century, television broadcasting shifted from analog to digital. Several analog microwave point-to-point link and analog satellite-television antennas were decommissioned since no longer required by the new, more efficient digital modulations. The computing power of personal computers and corresponding interfaces increased to allow the comprehensive signal processing required for digital-television reception. Both allowed very successful radio-astronomical observations with amateur means [3], [4].

Radio astronomy excels in interferometry, especially VLBI. While smaller baseline interferometers could work with dedicated microwave point-to-point links, VLBI usually required sophisticated synchronization with atomic clocks and physical transfer of high-capacity magnetic-tape recordings for further processing. Today global navigation satellite systems (GPS, GLONASS and similar) offer precise worldwide synchronization. The fiber-optic network offers high-capacity worldwide internet connectivity. Since both inexpensive synchronization and inexpensive data transfer is available to amateurs, the major achievements of amateur radio astronomy are yet to come.

In this article the design, construction and calibration of a compact radio telescope is discussed in detail. The latter can produce 3D maps of the hydrogen distribution in our galaxy. Much of the described hardware and software can be used to observe other celestial sources, like point and distributed continuum sources, a few neighbor galaxies, some of the strongest pulsars etc. Finally, several such radio telescopes could be combined into a powerful interferometer.

2. Radio-telescope design

2.1. System requirements

The $\lambda=21\text{cm}$ neutral-hydrogen line is not emitted by dense celestial objects like stars, but by lone hydrogen atoms in the interstellar medium. The density of the interstellar medium in a galaxy may be very low, just a few thousand particles in a cubic meter of space. Most of them are hydrogen atoms that emit a single photon at the precise frequency of $f_0=1420405751.7667\text{Hz}$ corresponding to a spin-reversal energy transition every 11 million years.

Yet our Milky Way and other galaxies are very large objects. Although the interstellar space can be considered rather high vacuum, the few lone hydrogen atoms represent a significant fraction of the total mass of a galaxy or other celestial body. The mass ratio varies: there are celestial objects with lots of sparse hydrogen atoms and few visible stars and the opposite is also possible. Due to the huge size of interstellar space, the radiation at $\lambda=21\text{cm}$ sums up to significant and detectable values.

Since relative velocities between different parts of our Milky Way galaxy span up to $\Delta v \approx \pm 200\text{km/s}$, the expected Doppler shift is in the range of $\Delta f \approx \pm 1\text{MHz}$ around a central frequency of $f_0 \approx 1420.4\text{MHz}$. Other galaxies are moving at even higher velocities with respect to us resulting in much larger Doppler shifts. Most important of all, the Doppler shift of the hydrogen line allows precise velocity measurements revealing the motions of celestial objects. The frequency band from $f_{MIN}=1400\text{MHz}$ to $f_{MAX}=1427\text{MHz}$ is therefore protected worldwide for radio-astronomy use.

The $\lambda=21\text{cm}$ neutral-hydrogen radiation from the Milky Way is coming from distributed sources with angular diameters of several degrees and an equivalent back-body brightness temperature of up to $T \approx 100\text{K}$. Such sources can be reliably detected with rather small antennas with a diameter above $d > 1\text{m} \approx 5\lambda$. Using a slightly larger antenna $d \approx 3\text{m} \approx 15\lambda$ already reveals the spiral structure of the Milky Way.

The receiving system of any radio telescope should add the lowest possible own noise to the weak celestial signals. The receiving system noise includes the antenna noise and the receiver electronics noise. The antenna noise mainly comes from unwanted side lobes of its radiation pattern picking up thermal radiation of the warm neighborhood. Modern semiconductor devices produce a similar amount of noise when operated at room temperature. The sum of both is in the range $T_s = 50\ldots 100\text{K}$ for relatively small antennas $d \approx 15\lambda$ and available low-noise amplifiers.

2.2. Block diagram

The design of the described compact radio telescope is based on available components: a 3.1m (10 feet) diameter surplus parabolic mesh reflector originally manufactured by EchoStar and intended for satellite-television reception in the 4GHz band. The parabolic dish is installed on an EGIS azimuth/elevation rotor EPR-203. Its corresponding control unit EPS-103 allows computer control through an RS-232 interface. A convenient solution is to run Python scripts on a personal computer to track a selected object in the sky and/or scan the galactic plane as shown on Figure 1:

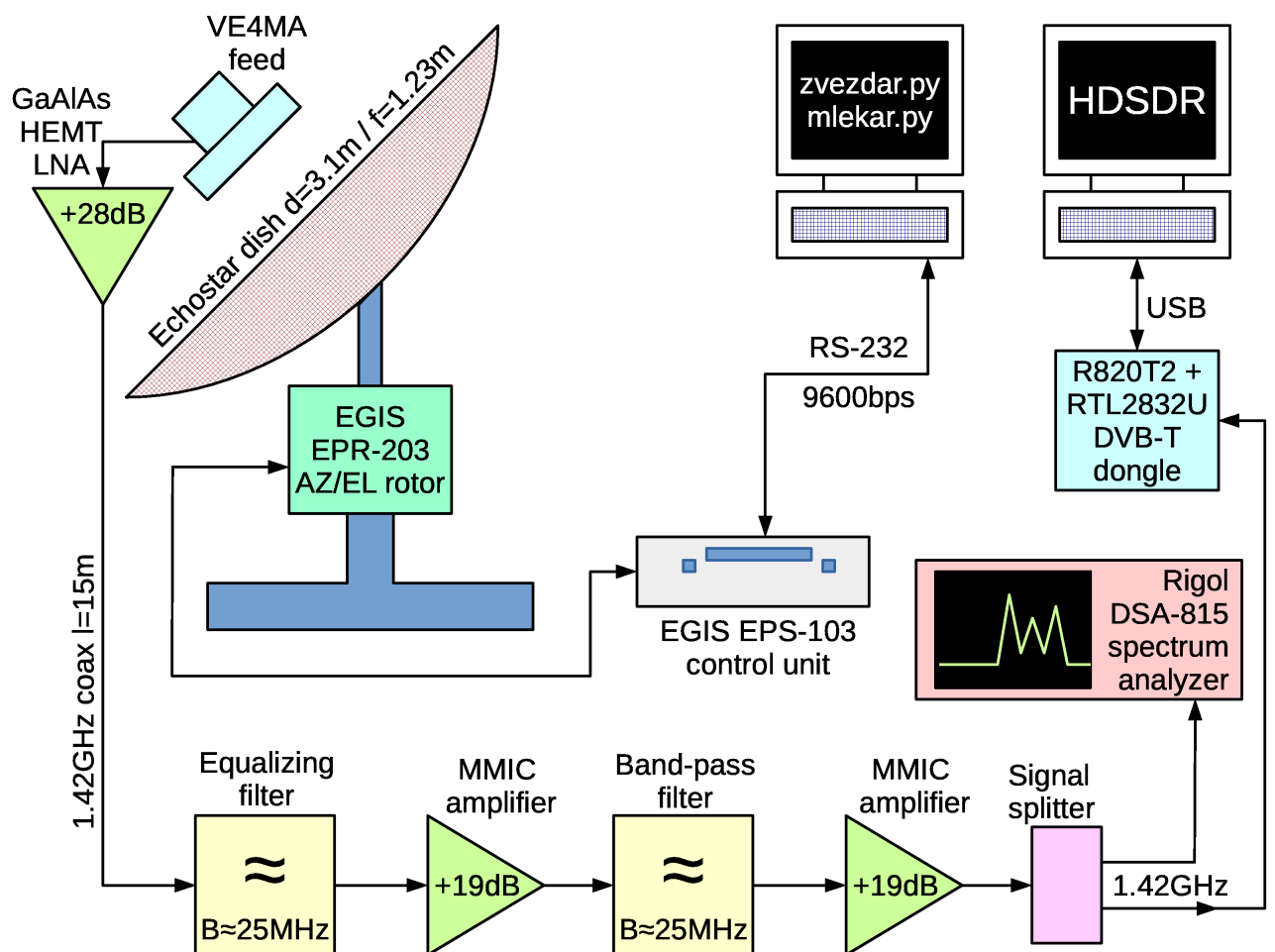


Figure 1: Block diagram of a compact hydrogen-line radio telescope.

Other parts of the radio telescope have to be custom designed and built. The VE4MA antenna-feed design is a good compromise among parabolic-mirror illumination efficiency, unwanted side lobes picking up noise and aperture blocking. Of course, the best available HEMTs have to be used in the low-noise amplifier. Since 1.42GHz is not a particularly high frequency for

modern electronics, frequency conversions are not required. The custom signal processing only includes custom-designed band-pass filters for 1.42GHz and additional amplifiers to overcome the relatively high noise of available receivers.

Further signal processing is split into two independent branches. A quick look at the received signal as well as interference threats is provided by a standard, scanning-receiver type spectrum analyzer Rigol DSA-815. Much more efficient signal processing can be performed with a FFT spectrum analyzer once the wide dynamic range of a scanning-receiver spectrum analyzer is no longer required. FFT spectrum analysis can be performed efficiently on modern personal computers using an inexpensive DVB-T dongle as the analog interface.

2.3. Antenna and positioner

The antenna of a radio telescope requires an unobstructed view to a much larger part of the sky than a typical satellite-television antenna covering the geostationary arc. In particular, on the northern hemisphere a radio telescope should have an unobstructed view in the direction south. It therefore makes sense to install a small radio telescope on the roof or other elevated place to avoid local obstacles as shown on Figure 2:



Figure 2: Mesh reflector with feed, LNA and azimuth/elevation positioner.

The spatial resolution of any radio telescope depends on the antenna size. Assuming an uniform illumination of the antenna aperture, the spatial resolution of the described single-antenna radio telescope is estimated as:

$$\alpha = 1.22 \cdot \frac{\lambda}{d} = 1.22 \cdot \frac{0.21\text{m}}{3.1\text{m}} = 0.083\text{rd} \approx 4.7^\circ$$

In the case of a radio telescope, the antenna requires two-axis rotation. An azimuth/elevation or X/Y rotator can be used to keep the antenna pointed to a particular source in the sky in spite of the rotation of the Earth. On the other hand, the rotation of the Earth is frequently used in many radio-telescope designs as an additional axis of rotation. In the described radio telescope, all three available axis of rotation (two-axis positioner and Earth) can be used depending on the desired scan operation. The EGIS azimuth/elevation rotor EPR-203 is equipped with gears for 360° azimuth range and 90° elevation range.

2.4. Feed design

In the microwave frequency range, the sky noise is usually much lower than the ground noise. The equivalent black-body temperature of the sky may be less than $T_{SKY} < 10K$ while the ground noise is close to $T_{GROUND} \approx 290K$. Large satellite-receiving antennas and radio telescopes are designed to avoid collecting ground noise through side lobes of their radiation patterns. Antennas larger than $d > 100\lambda$ are typically built as dual-reflector Cassegrain telescopes. In this way any spillover of the feed sees the cold sky over the edge of the secondary reflector.

An alternative solution is to control the radiation pattern of the feed using a corrugated horn or a corrugated flange. Neither solution is practical with small, rotational-symmetric parabolic mirrors due to the blockage of the relatively large secondary mirror or corrugated feed. An efficient solution for small $d < 30\lambda$ parabolic mirrors is a simple circular-waveguide horn with the Kumar choke [5], also known as the VE4MA feed [6] as shown on Figure 3:

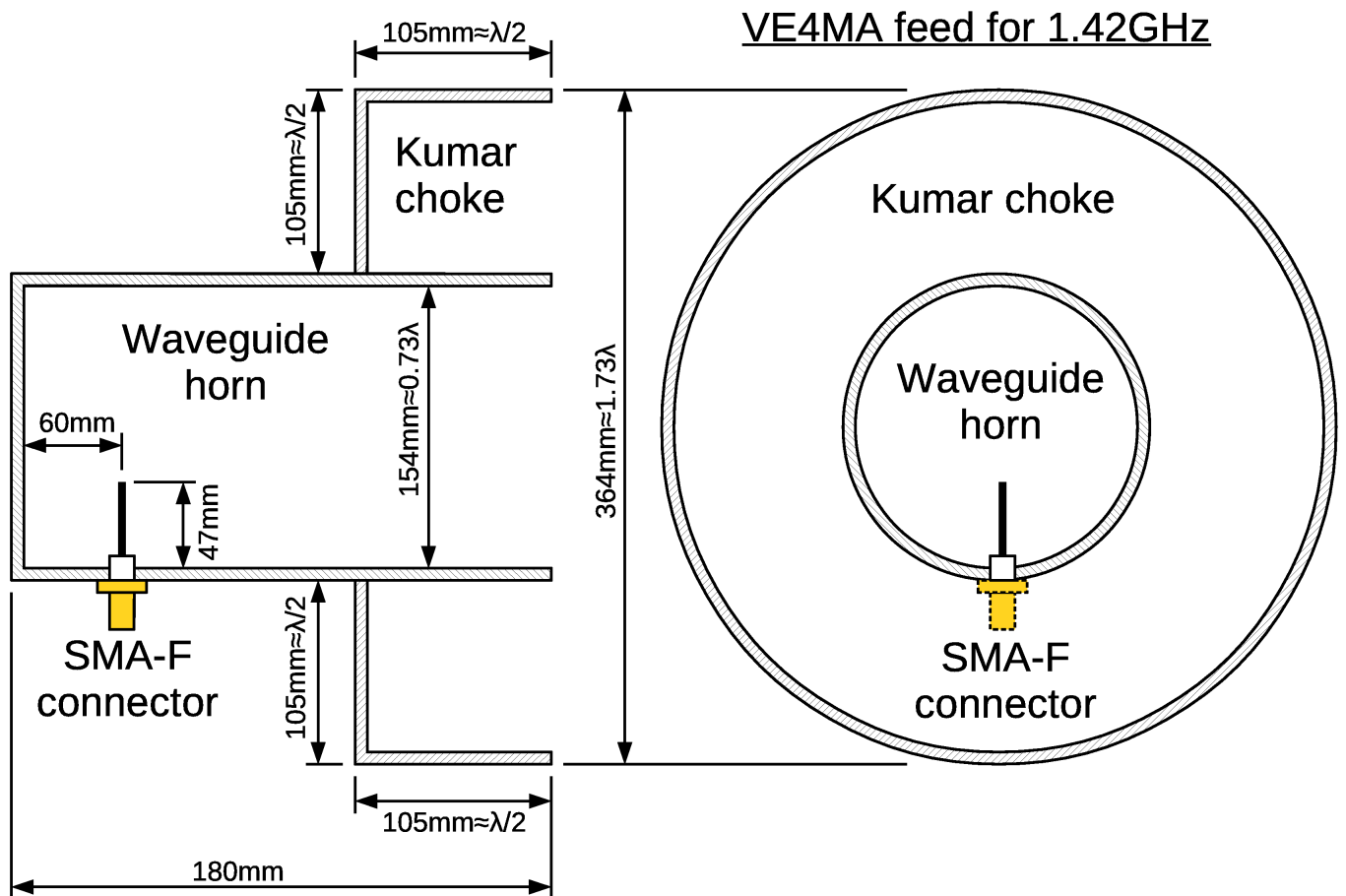


Figure 3: VE4MA feed design.

Changing the diameter of the circular waveguide, the dimensions of the Kumar choke as well as its position relative to the horn aperture allows optimizing the VE4MA feed for deep, rotational-symmetric parabolic mirrors with focal-to-diameter ratios in the range $f/d = 0.3...0.5$. The dimensions shown on Figure 3 should be close to optimal for our EchoStar mesh dish with a

focal-to-diameter ratio of $f/d=0.4$ at a central frequency of $f_0=1.42\text{GHz}$.

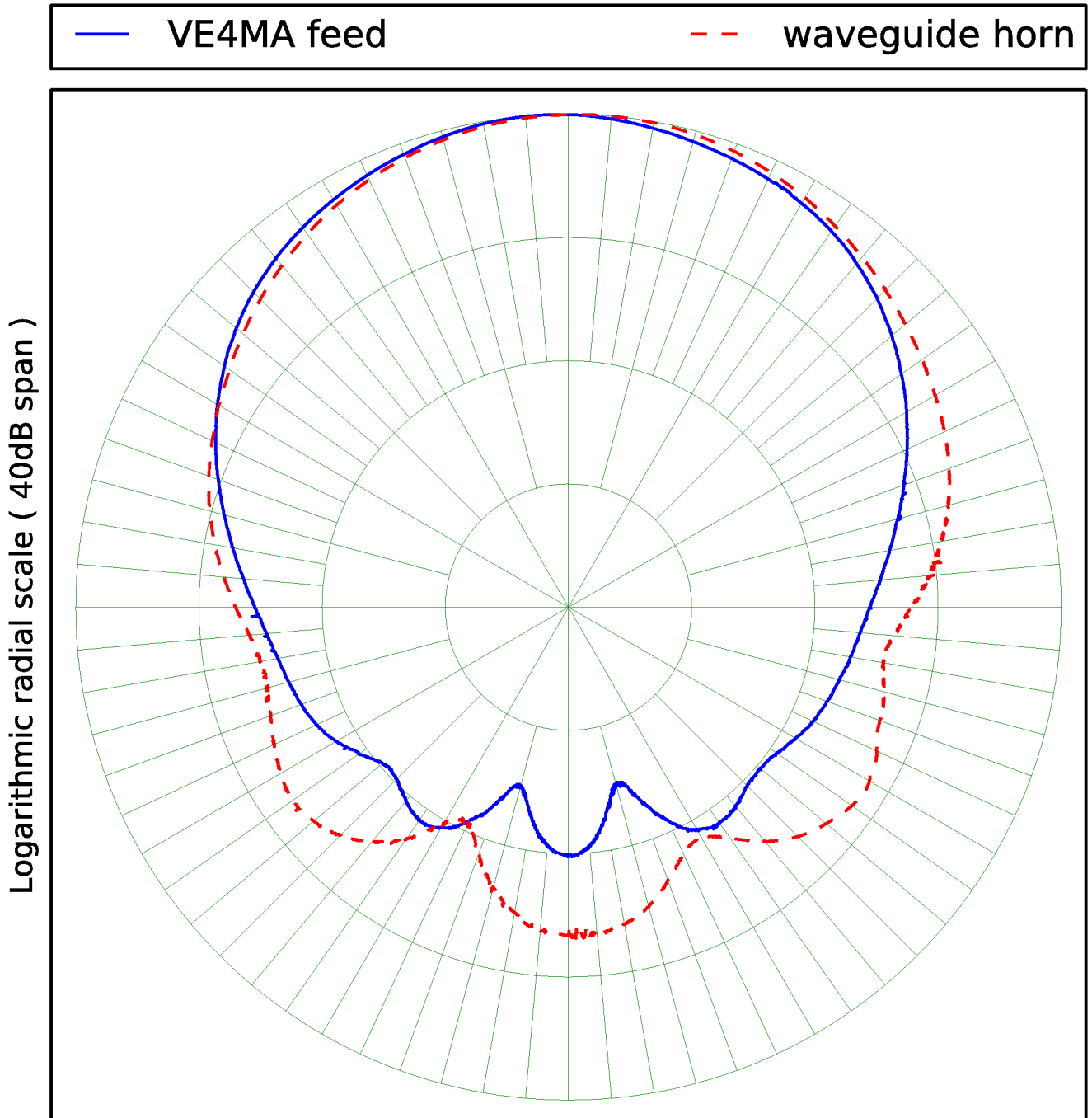
The described VE4MA feed was practically implemented from pieces of thin aluminum sheet bolted together with several M3 screws as shown on Figure 4. The position of the Kumar choke with respect to the horn aperture was adjusted experimentally for the lowest system noise temperature T_s :



Figure 4: Practical implementation of the VE4MA feed.

The efficiency of the Kumar choke was further checked by measuring the radiation pattern of the feed both with the Kumar collar and the bare waveguide horn with the choke removed. The measurements also show important side effects that might impair the performance of the radio-telescope antenna.

For example, a circular waveguide only supports the propagation of its fundamental TE_{11} mode when its diameter exceeds $d_{\text{TE}11}>0.586\lambda$. Using a simple, non-symmetric probe to excite the fundamental TE_{11} mode, higher order modes may also be excited. The next higher mode is the TM_{01} mode that appears at $d_{\text{TM}01}>0.765\lambda$. Since the circular-waveguide diameter was selected as $d=0.73\lambda$ rather close to the TM_{01} cutoff, the latter does not receive much attenuation in a short waveguide horn. The final result is a squint of the waveguide-horn main radiation lobe in the E plane. Fortunately the Kumar choke in the VE4MA feed is able to correct this defect as shown on Figure 5:

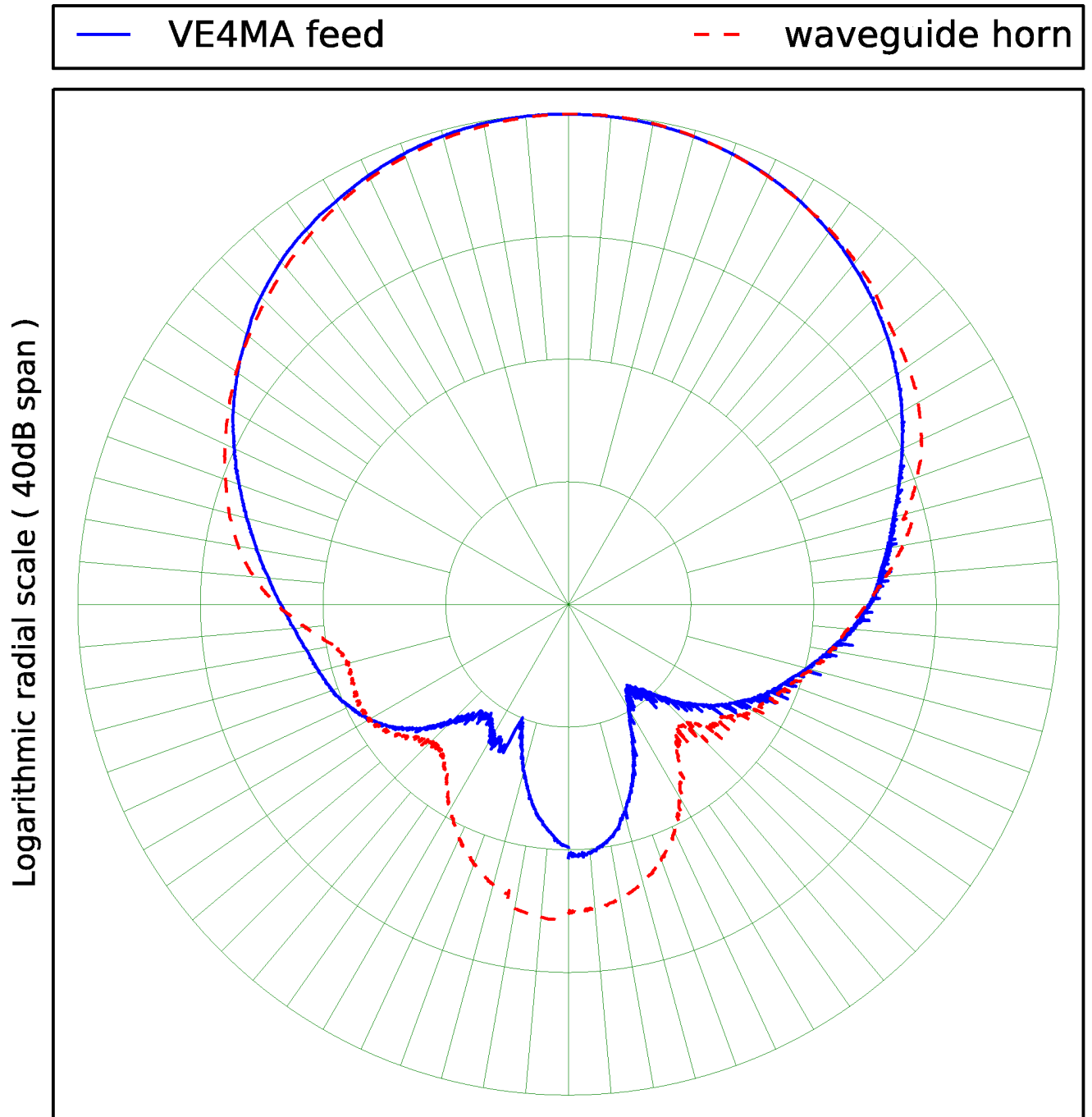


E-plane radiation pattern

VE4MA feed -3dB Beamwidth: 76.6 Directivity: 6.8 = 8.34 dBi
 waveguide horn -3dB Beamwidth : 75.2 Directivity: 5.6 = 7.52 dBi

Figure 5: Measured feed E-plane radiation pattern.

Little if any squint is visible in the measured H-plane radiation pattern of the bare waveguide horn as compared to the VE4MA feed on Figure 6:



H-plane radiation pattern

VE4MA feed -3dB Beamwidth: 72.6 Directivity: $7.5 = 8.75 \text{ dBi}$
 waveguide horn -3dB Beamwidth : 70.2 Directivity: $7.2 = 8.59 \text{ dBi}$

Figure 6: Measured feed H-plane radiation pattern.

In both E and H planes, the Kumar choke provides a substantial improvement of the feed radiation pattern resulting in a more than 5dB decrease of its unwanted side lobes. Further, the VE4MA feed exhibits a much better rotational symmetry than the bare waveguide horn. The improved feed radiation pattern allows a substantially lower system noise as measured during the calibration in section 3.2. of this article.

The radio emissions of certain celestial sources are polarized, while radio emissions from other celestial sources are not polarized. The radio emission of neutral hydrogen atoms at $\lambda=21\text{cm}$ is not polarized. Therefore the polarization of a simple radio telescope for the neutral-hydrogen line may be arbitrary. The simplest solution is to use linear polarization as with the described linearly-polarized VE4MA feed. Both horizontal linear polarization and vertical linear polarization were experimented with identical results.

While using linearly-polarized feeds with relatively small $d < 30\lambda$, rotational-symmetric

parabolic mirrors, a new problem appears. A significant part of the feed radiation is reflected by the parabolic mirror back into the same feed. Considering the described mesh dish with a focal $f=1.23\text{m}$ and the described VE4MA feed with a gain of about $G \approx 8.55\text{dBi} \approx 7.15$ at $\lambda=21\text{cm}$, the magnitude of the described reflection can not be neglected:

$$|\Gamma| = \frac{G \cdot \lambda}{4\pi \cdot f} \approx 0.097 \approx -20.3\text{dB}$$

This additional reflection may either degrade or improve the feed impedance matching, since the overall antenna return loss is a phasor sum of the different reflections involved. On the other hand, the noise performance of very low-noise microwave receivers is very sensitive to the source (antenna) impedance matching. Some low-noise receivers may even become unstable when connected to a badly mismatched antenna.

The return loss of the described bare VE4MA feed in free space was measured as $|\Gamma|=-13.4\text{dB}$ using a directional coupler with a measured directivity better than -30dB . After installing the feed in the focal point of the parabolic mirror, the return loss of the whole antenna improved to $|\Gamma|=-17.8\text{dB}$ at $f_0=1.42\text{GHz}$. This return loss was considered good enough so that any further modifications to the feed were considered unnecessary.

The above discussion is no longer valid if a parabolic mirror with a different focal length from ours is used, since the phase of the reflection from the dish changes really quickly and is proportional to twice the focal length! Using an arbitrary parabolic mirror, the impedance matching of the complete antenna should always be checked. In the worst case, the feed design, in particular the probe length and its position inside the waveguide horn may need to be changed.

2.5. LNA design

The semiconductor devices of choice for microwave low-noise amplifiers (LNAs) are high-electron mobility transistors (HEMTs) based on GaAs. The best commercially-available devices are designed to operate in a $Z_K=50\Omega$ characteristic-impedance environment in the frequency range around $f_0=12\text{GHz}$ for satellite-television reception. Such devices are therefore not optimized for operation at the neutral-hydrogen frequency of $f_0=1.42\text{GHz}$.

Similar HEMT structures with a much wider gate are required for low-noise operation in a $Z_K=50\Omega$ environment at L-band frequencies. Besides not being volume-production items, wider-gate devices operate at higher currents increasing the power dissipation. The latter increases the chip temperature impairing their noise performance. It therefore makes sense to use standard 12GHz HEMT devices even at much lower frequencies but in a higher-impedance environment as described in [7].

The circuit published in [7] was originally designed for GaAs MESFETs that operated at about $V_{DS} \approx 4\text{V}$. Modern low-noise GaAlAs/GaAs HEMTs operate at much lower voltages $V_{DS} \approx 1.5\text{V}$. Operation of a low-noise HEMT at higher voltages may affect its reliability and trigger long-term degradation effects. In order to improve the reliability with HEMT devices, the simple source-bias resistor from [7] was replaced with an active bias circuit including a low-frequency silicon NPN transistor.

When a Ku-band HEMT or MESFET is operated at L band, an efficient input-impedance match for lowest noise is a series inductor with the gate while no special output-impedance matching at the drain is required. A two-stage amplifier design offers around $G_{LNA} \approx 30\text{dB}$ of gain at reasonable stability. Both gain and stability can be adjusted with the inter-stage match. A GaAs MESFET can be used in the second stage as shown on Figure 7:

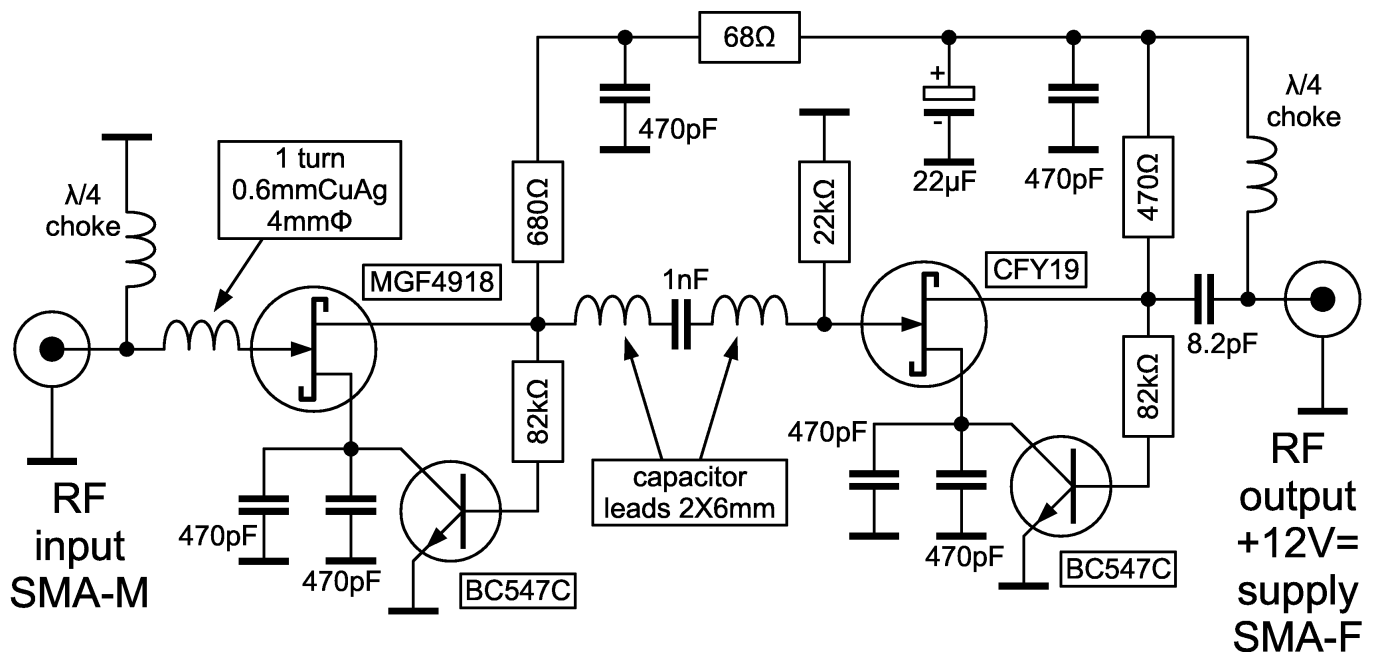


Figure 7: LNA circuit diagram.

In order to operate at higher impedances, the circuit of the LNA is not built on a printed-circuit board. The circuit of the LNA is supported in free air by several lead-less 470pF ceramic disc capacitors soldered to the bottom of a small brass box. The remaining components are traditional parts (not SMD) with wire leads. Although such a design is not suitable for volume production, it makes sense to achieve top performance of the radio telescope. The supply voltage +12V= is fed through the output SMA connector using a bias tee at the other end of some 15m of coaxial cable feeding the indoor equipment. The input connector is a male SMA to be screwed directly on the antenna feed to avoid any feed-line losses as shown on Figure 8:



Figure 8: Practical implementation of the LNA.

Many LNA prototypes were built using different GaAs devices either in the original circuit [7] or with the modified bias as shown above. Both MESFETs and HEMTs could readily achieve noise temperatures in the $T_{LNA} \approx 30K$ range as measured with a HP8970 noise-figure meter equipped with a HP364A $ENR \approx 5dB$ calibrated noise source. The best LNA samples could reach even

$T_{LNA} = 25K$ at a room temperature of 20°C (293K) after carefully adjusting the input impedance match. HEMTs typically provide much more gain than MESFETs, therefore using HEMTs in both stages may lead to instability.

The LNA is followed by the indoor receiver with a noise temperature in the $T_{RX} \approx 290K$ (room temperature) range. Considering an $a_{COAX} = -10dB$ cable loss to the rooftop antenna and a LNA gain of $G_{LNA} \approx 30dB$, the indoor receiver adds about $T_{RX}' \approx 3K$ of noise to the whole radio telescope noise temperature.

2.6. Signal processing and distribution

A carefully-designed LNA may contribute less than $T_{LNA} \approx 30\text{K}$ to the total system noise of the radio telescope, but other components may be much noisier. For example, a good radio-frequency spectrum analyzer has a noise figure in the $F_{SA} \approx 25\text{dB}$ range corresponding to a noise temperature of about $T_{SA} \approx 10^5\text{K}$. A $G_{LNA} \approx 30\text{dB}$ LNA followed by $a_{COAX} = -10\text{dB}$ cable loss sets the contribution of the spectrum analyzer to an unacceptable $T_{RX}' \approx 1000\text{K}$ to the total system noise or in other words more than one order of magnitude larger than any other noise source in the system.

Additional low-noise amplification is therefore required in front of spectrum analyzers and other "deaf" instrumentation. Additional amplification brings a new problem: a high-gain amplifier chain may easily be driven into saturation by strong terrestrial radio transmitters operating at nearby frequencies. The whole signal processing and distribution chain includes a bias tee for the LNA, a first band-pass filter, a MMIC amplifier, another band-pass filter, another MMIC amplifier, a power splitter and a SDR receiver front-end as shown on Figure 9:

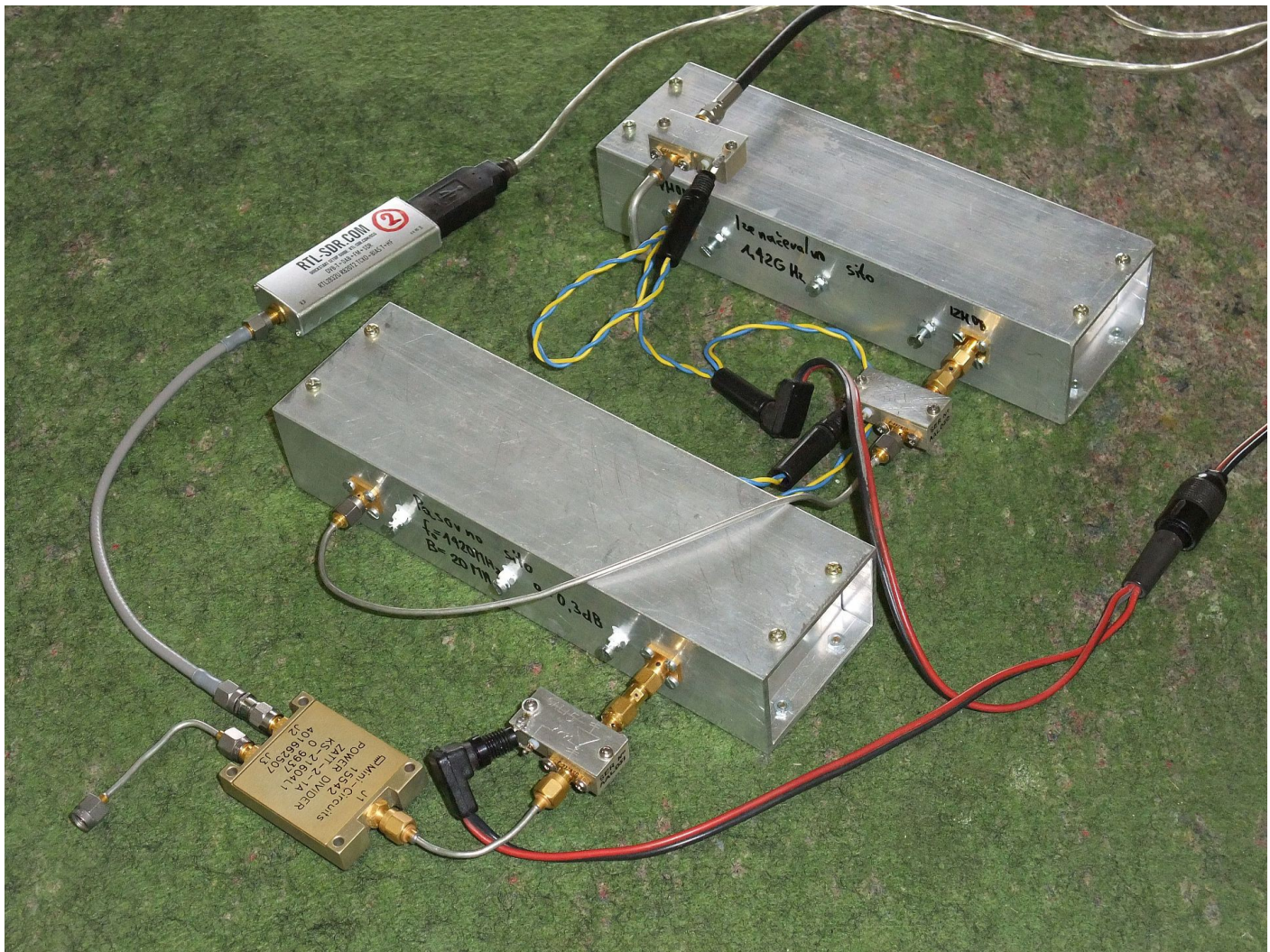


Figure 9: Signal processing and distribution chain.

Microwave filters can be built in many different technologies. For the radio-astronomy frequency band at 1.42GHz any filters have to be custom designed and built therefore excluding high-volume technologies like SAW devices. Considering low-volume applications, cavity filters are simple to manufacture from standard aluminum tubing yet individual $\lambda/4$ resonators achieve an unloaded quality in excess of $Q_u > 1000$. A comb arrangement of the individual $\lambda/4$ resonators allows a more compact band-pass filter than an interdigital design. Considering the the

filtering requirements of the radio telescope, two separate but almost identical comb filters with three $\lambda/4$ resonators each are required as shown on Figure 10:

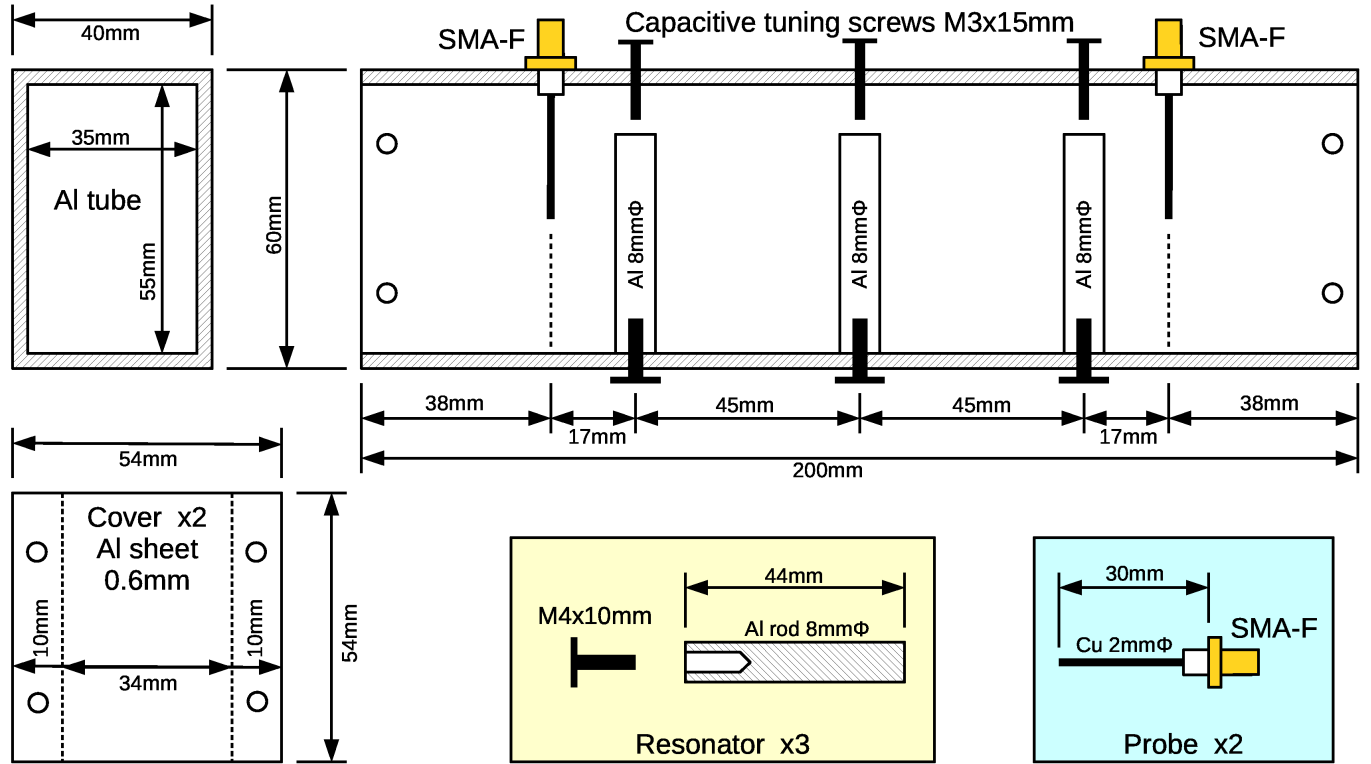


Figure 10: Comb-filter design.

The input and output coupling is achieved with probes similar to the one used to excite the waveguide horn. The three resonators are made from 8mm diameter aluminum rod, while the cavity is made from standard aluminum tube of rectangular cross-section of 40mmX60 and 2.5mm thick walls. The rectangular tube extends 38mm beyond the probe positions so that the electromagnetic field already decays inside the tube. Covers on both sides of the filter cavity as shown on Figure 11:

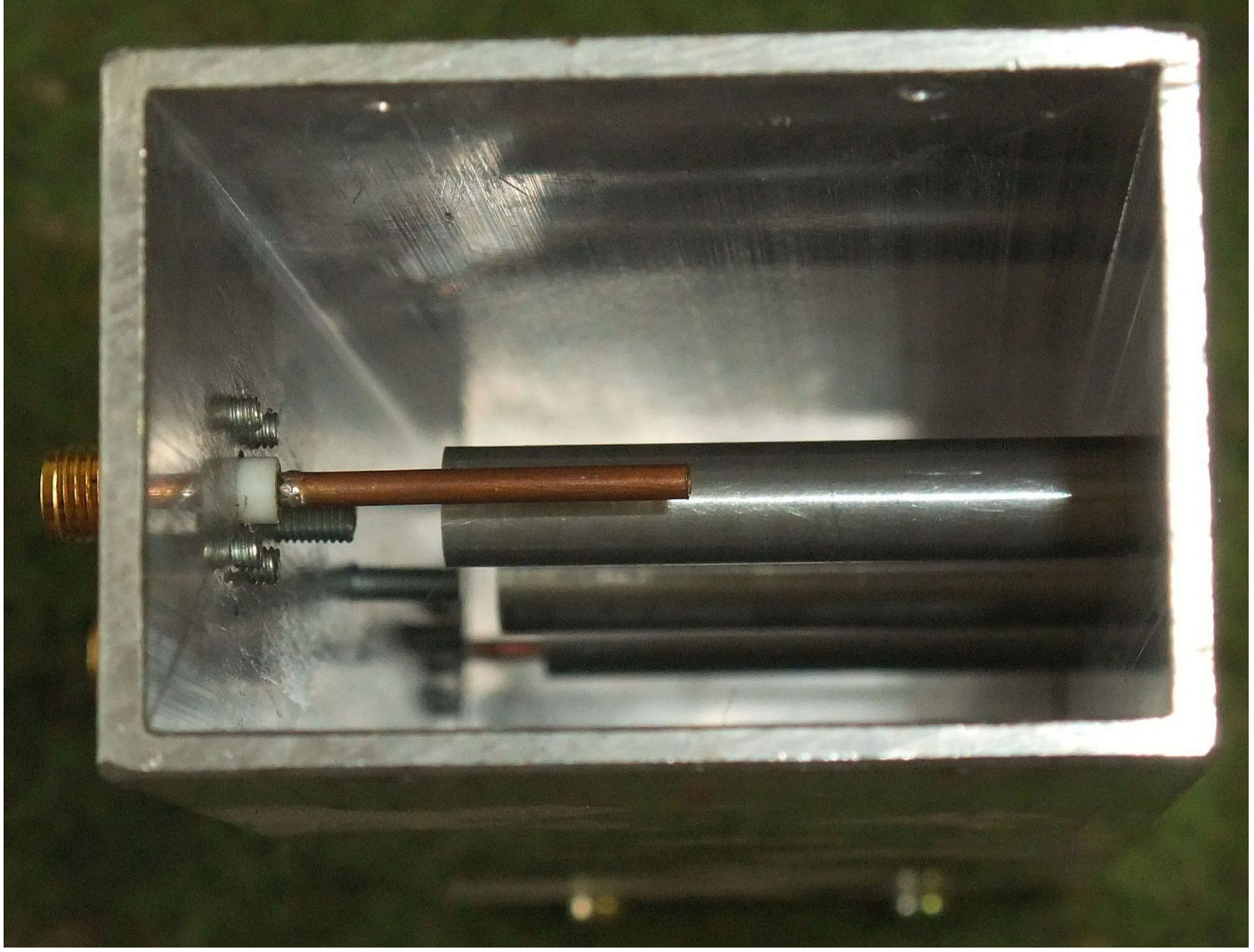


Figure 11: Inside the comb-filter cavity.

The described simple all-aluminum construction with few junctions provides excellent electrical performances that stay stable in time. The $\lambda/4$ resonators are tuned to the exact frequency with capacitive tuning screws in the opposite wall of the cavity. The bandwidth is selected to cover the whole 1.42GHz radio-astronomy frequency band. An order-of-magnitude narrower filter could be used to observe the neutral-hydrogen radiation only from our Milky Way galaxy.

At a pass-band bandwidth of $B \approx 25\text{MHz}$ the high unloaded quality of the individual resonators allows a low insertion loss of the whole three-stage filter in the $a_{BPF} \approx -0.5\text{dB}$ range. The exact value of the latter is a function of the actual filter alignment as visible on the measured response on Figure 12:

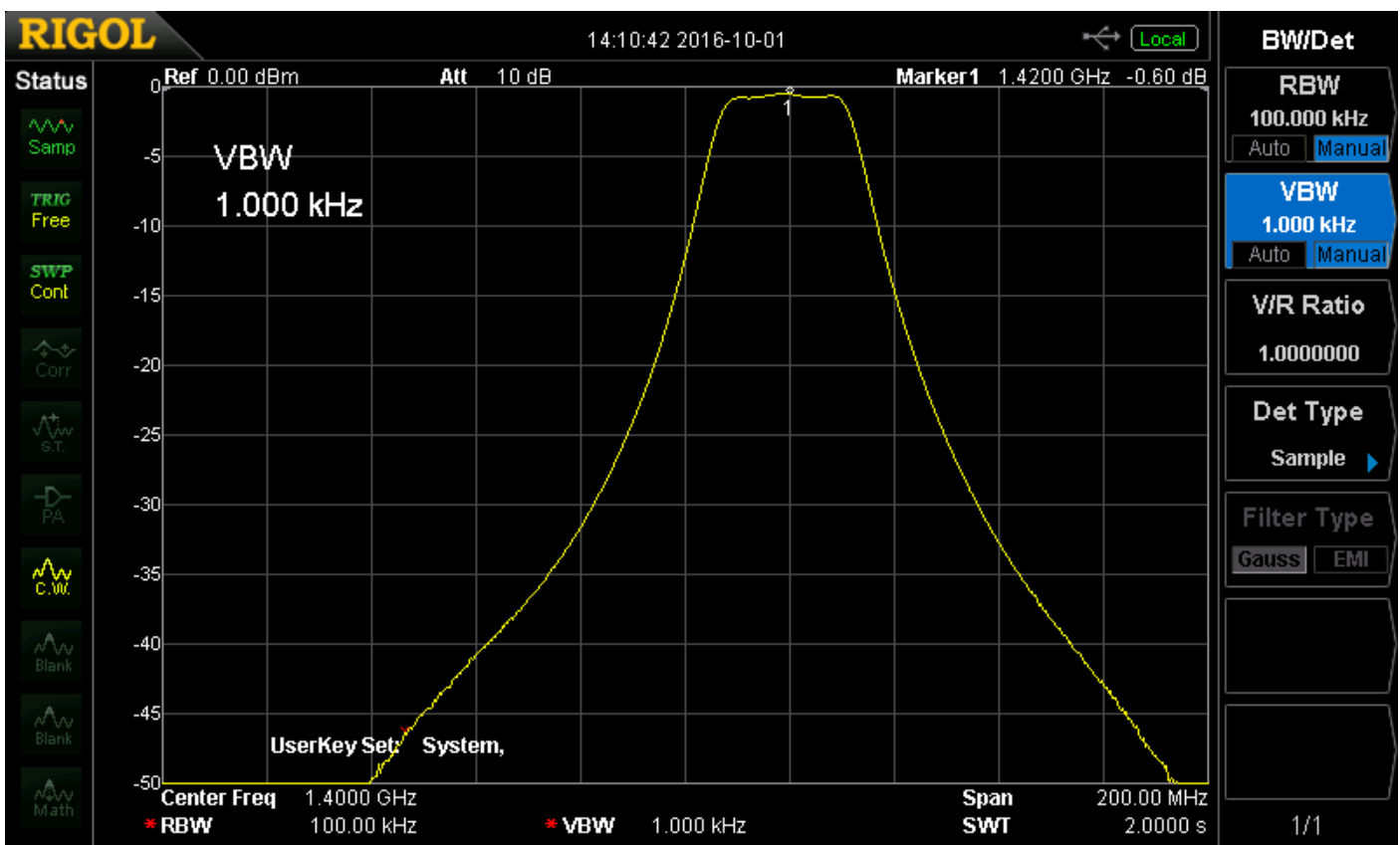


Figure 12: Measured comb-filter response.

Unfortunately, other components of the radio telescope do not exhibit such a flat frequency response over the 1.42GHz radio-astronomy band. Since most of the ripple comes from the reflections at both ends of the relatively long coaxial cable between the outdoor LNA and the indoor processing chain, it makes sense to adjust the first cavity filter to flatten the overall frequency response of the radio telescope. In this way the first filter is also used as an equalizing filter.

The additional signal gain is provided by two MMIC amplifiers manufactured by Mini-Circuits in InGaP HBT technology. The amplifier chips are packaged in SOT-89 plastic packages that provide good radio-frequency and thermal performance at the same time. Both packaged amplifiers are installed on printed-circuit boards together with a few bias components. Finally both printed-circuit boards are installed in aluminum cases with SMA connectors as shown on Figure 13:

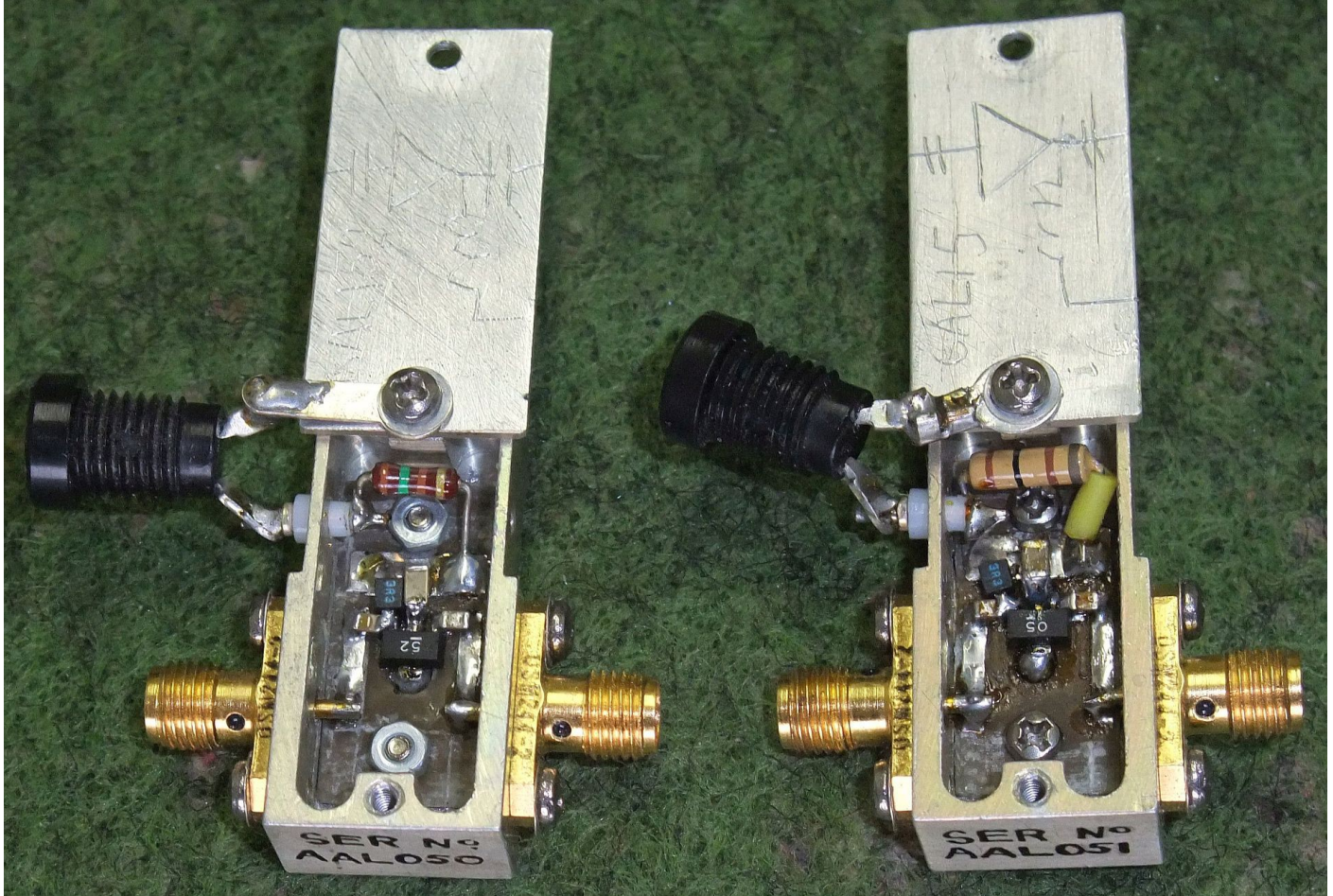


Figure 13: Packaged MMIC amplifiers.

A low-noise MMIC Gali-52+ is used in the first stage providing a measured gain of $G_{52}=19.3\text{dB}$ with a measured noise figure of $F_{52}=2.8\text{dB}$ in the 1.42GHz band. A power MMIC Gali-5+ is used in the second stage providing a measured gain of $G_5=19.1\text{dB}$ with a measured noise figure of $F_5=4.1\text{dB}$ in the 1.42GHz band.

The gain of the whole chain including two band-pass filters and two MMIC amplifiers approaches $G \approx 37\text{dB}$. The latter is high enough to neglect the noise contribution of a spectrum analyzer or software-defined radio (SDR) front end. A Wilkinson power divider with a splitting loss of $a_w \approx -3\text{dB}$ is used to supply two independent instruments at the same time.

3. Instrument calibration

3.1. Positioner calibration

No matter what directional antenna and corresponding positioner are used, after installation both need accurate mechanical calibration before they can be used for satellite communications and/or radio-astronomy work. In particular, the available EGIS azimuth/elevation rotor EPR-203 has a linear tooth-gear transmission for rotation in the azimuth plane and a non-linear worm-gear-plus-lever transmission for rotation in the elevation plane. The azimuth calibration is simply finding the offset constant from the reference position due to installation and rotor errors. Once found, the offset constant may simply be inserted in the corresponding EGIS control unit EPS-103.

The non-linear elevation transmission of the EGIS rotor EPR-203 is much more tricky. The look-up table correction built in the EPS-103 control unit was found rather inaccurate. Adjusting the remaining elevation offset constant did not solve the problem. A working solution was to derive our own elevation-correction table in 5-degree steps using a gravity inclinometer as shown on Figure 14:



Figure 14: Using the inclinometer.

Finally, linear interpolation between two neighbor correction-table points is implemented in the Python code controlling the antenna positioner.

The inclinometer is further used to correct small installation errors. The supporting mast of the antenna was found to deviate as much as one degree from vertical. Rather than performing mechanical adjustments on the antenna and/or its support structure, such small errors are easily corrected in Python code as vector rotations.

The final check of the antenna/rotor alignment is tracking the Sun. The position of the latter can be computed precisely at any time. The Sun is the strongest natural source of radio waves in the sky. Of course the Sun can be tracked optically, for example by checking the position of the feed shade on the parabolic reflector. Using rotational-symmetric parabolic reflectors, the feed shade should fall exactly in the center of the dish as shown on Figure 15:



Figure 15: Checking the feed shade.

3.2. System noise temperature

A very important parameter of any satellite-receiving station and/or radio telescope is the system noise temperature. The latter describes the amount of noise added by the station hardware to the received signal. The simplest procedure to measure the system noise temperature is to turn the antenna into two different targets radiating as black bodies at well known temperatures. The described hot/cold method yields the hot/cold power ratio:

$$Y = \frac{P_{HOT}}{P_{COLD}} = \frac{B \cdot k_B \cdot (T_{HOT} + T_s)}{B \cdot k_B \cdot (T_{COLD} + T_s)} = \frac{T_{HOT} + T_s}{T_{COLD} + T_s}$$

Both the receiver bandwidth B and the Boltzmann constant $k_B \approx 1.38 \cdot 10^{-23} \text{ J/K}$ cancel out in the hot/cold ratio. The radio-telescope antenna is first pointed to a cold part of the sky assuming $T_{COLD} \approx 10\text{K}$. The antenna is afterwards pointed to a forest (good microwave absorber if dry) assuming $T_{HOT} \approx 290\text{K}$. The described radio-telescope with the VE4MA feed achieved a hot/cold ratio $Y \approx 7\text{dB} \approx 5$. The measured system noise temperature is:

$$T_s = \frac{T_{HOT} - Y \cdot T_{COLD}}{Y - 1} = \frac{290\text{K} - 5 \cdot 10\text{K}}{5 - 1} = 60\text{K}$$

It is estimated that these 60K include about 32K coming from the LNA, about 3K coming from the remaining stages of indoor signal processing and about 25K from the antenna side lobes observing the warm Earth. Such a low antenna noise temperature of just 25K is an excellent result for the VE4MA feed and a relatively small $d \approx 20\lambda$ parabolic dish obstructed by the feed itself

and its four metal supporting struts.

For comparison, the same measurement was also performed with the a simple waveguide-horn feed by removing the Kumar choke from the VE4MA feed. A hot/cold ratio of only

$Y \approx 5\text{dB} \approx 3.16$ was obtained in the latter case. The corresponding measured system noise temperature doubled to $T_s \approx 120\text{K}$ therefore halving the sensitivity of the radio telescope! Removing the Kumar choke therefore increases the antenna temperature up to 85K due to the much larger side lobes of a simple waveguide horn.

3.3. Antenna illumination efficiency

Yet another important parameter to check is the antenna aperture illumination efficiency. The latter may be impaired both due to an incorrect illumination (usually under-illumination) and/or due to mechanical defects of the parabolic-reflector surface. Neither can be detected with distributed sources like those used in the system-noise-temperature measurement described in the previous chapter.

A calibrated point source of radiation is required to measure the antenna aperture illumination efficiency. The Sun is a strong natural radio source. The Sun is small enough to be considered a point source since its angular diameter $\alpha_{SUN} \approx 0.5^\circ \ll \alpha \approx 4.7^\circ$ is much smaller than the resolution of the described radio telescope. Unfortunately the radio radiation from the Sun is changing with the Sun activity. Changes are different at different frequencies.

Fortunately for our measurement the activity of the Sun is monitored by several observatories around the world on many different frequencies. This data is regularly published on the internet like [8]. In our case the most useful observation is at $f_0 = 1415\text{MHz}$ and the most useful observatory is located in San Vito dei Normanni near Brindisi in Italy. The latter provides Sun data close to our local noon with the Sun high on the sky.

During our measurement San Vito reported a solar-flux spectral density of $S/B = 69\text{SFU} = 69 \cdot 10^{-22} \text{W/m}^2/\text{Hz}$ at $f_0 = 1415\text{MHz}$. At the same time we measured a hot/cold ratio of $Y \approx 13.5\text{dB} \approx 22.4$ while pointing the radio telescope both to the Sun and to a cold part of the sky. Considering that our antenna only receives half of the reported radiation on one polarization and that the cold sky radiates at $T_{COLD} \approx 10\text{K}$ we obtain the effective area of our antenna as:

$$A_{eff} = \frac{2 \cdot k_B \cdot (Y - 1) \cdot (T_s + T_{COLD})}{S/B} \approx \frac{2 \cdot 1.38 \cdot 10^{-23} \text{W/Hz/K} \cdot (22.4 - 1) \cdot (60\text{K} + 10\text{K})}{6.9 \cdot 10^{-21} \text{W/m}^2/\text{Hz}} \approx 5.99 \text{m}^2$$

Dividing the effective area with the physical area of our 3.1m parabolic dish we estimate the illumination efficiency as:

$$\eta = \frac{A_{eff}}{\pi \cdot (d/2)^2} \approx \frac{5.99 \text{m}^2}{\pi \cdot (3.1\text{m}/2)^2} \approx 0.79$$

An aperture illumination efficiency of 79% is an excellent result for a relatively small $d \approx 20\lambda$ parabolic dish obstructed by the VE4MA feed and its four metal supporting struts. This result also proves that the performance of our parabolic dish is not affected by mechanical distortions, at least at the given wavelength of $\lambda = 21\text{cm}$.

3.4. Radio-interference mitigation

An amateur radio-telescope builder usually has little if any choice to select the place where

to place his instrument. Wind is a primary concern for a large antenna. Snow and ice loading may also be important factors. While winds and precipitations have been observed and measured for many years, radio interference is a big unknown in a constantly changing world of electromagnetic pollution of any kind.

Traditional amateur astronomers usually prefer remote places to avoid optical pollution. Such places may have high winds and receive lots of precipitations in winter. An amateur radio telescope likely has to be placed in an urban environment where meteorological constraints are less severe. The level of radio interference in an urban environment may span over several orders of magnitude. Therefore at least some rough interference measurements are recommended in site before building such an instrument.

In our case the radio telescope is placed in a suburb of a town in a closed valley protected from winds. Interestingly, no radio interference from radio transmitters was found in the 1.42GHz protected astronomy band. The nearest radio transmission was found at about 1436MHz outside the protected band. It looks like certified radio transmitters are shielded and filtered enough not to cause harmful radio interference. As a precaution, a radio-frequency spectrum analyzer covering a 50MHz wide span around 1.42GHz is always connected to the radio telescope to check for interference as shown on Figure 16:

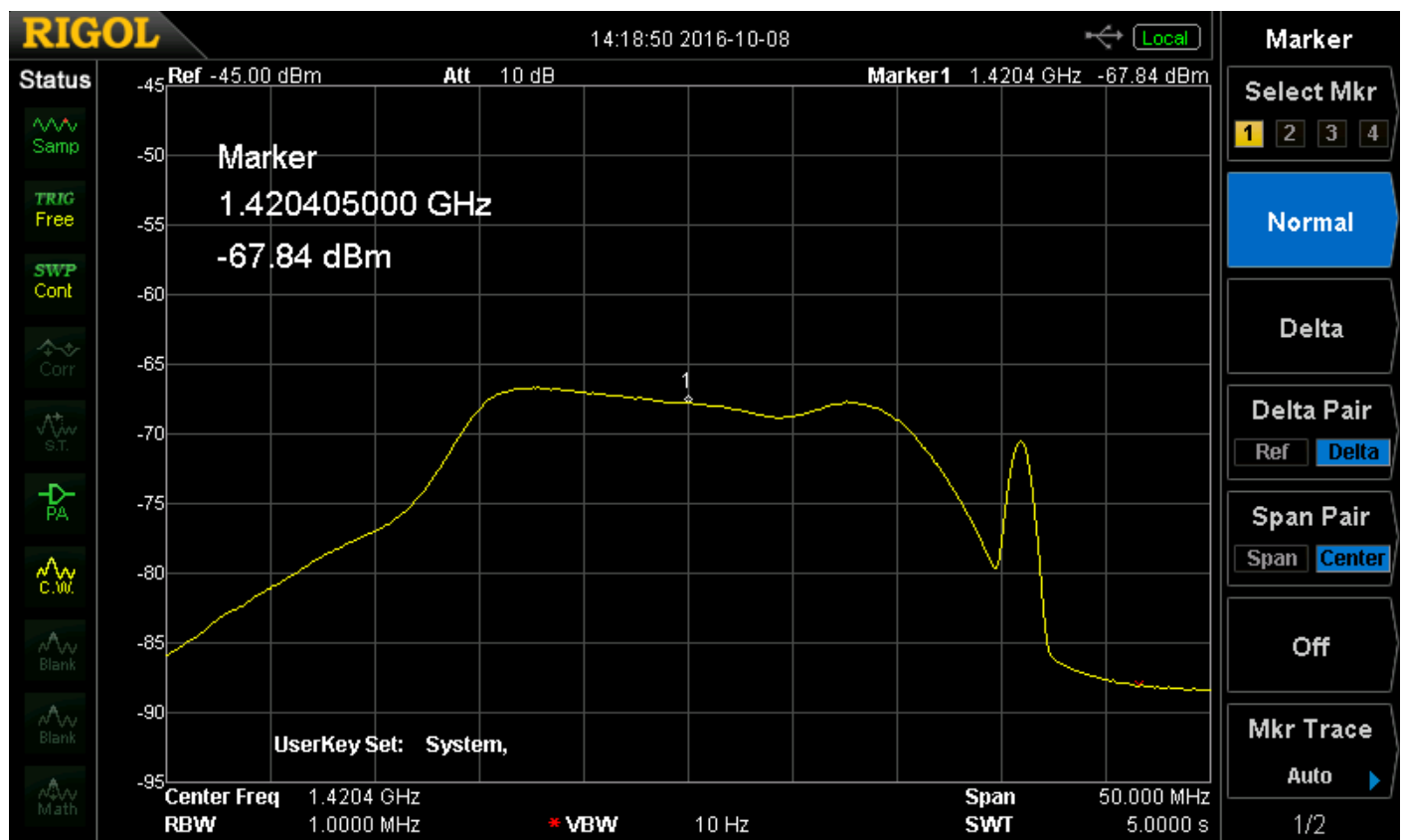


Figure 16: Pass-band around 1420.4MHz and interference at 1436MHz.

On the other hand, different kinds of radio interference were experienced from electronic and electrical equipment not intended to transmit any radio frequency at all. Live-video IP cameras from different manufacturers, cheap and expensive products alike, were identified as the worst source of radio interference, radiating harmonics of all clocks used by their internal digital circuits. Unlike suggested in many articles and websites, video IP cameras can not be used to help aiming the antenna of a radio telescope!

Most electronic equipment containing digital circuits causes narrow-band interference around 1420.000MHz +/- tolerances of their internal crystal oscillator. This interference may be a high-order harmonic of an internal clock operating at 10.000MHz or 20.000MHz. A simple countermeasure is to move all computers and network devices at least two concrete floors below the radio-telescope antenna. Such unintentional interference also decays quickly with distance. Of course all unnecessary electronic equipment may simply be switched off when the radio telescope

is operating...

Finally, we could not identify the source of some kind of wide-band interference that appears periodically. It may be coming from a spark-ignition system, most likely natural-gas heater, since its occurrence and period was found correlated with low outside temperatures. It should be noted that both narrow-band and wide-band low level interference could only be detected using software-defined-radio (SDR) techniques and very long integration times.

4. Hydrogen spectrum measurements

4.1. Spectrum analyzer

Our first experiments were performed with a conventional, scanning-receiver type spectrum analyzer Rigol DSA-815. Such an instrument has a better dynamic range than its all-digital FFT-based counterparts. On the other hand, a scanning receiver uses the incoming signal rather inefficiently. Most of the signal energy is lost while the scanning receiver dwells on other frequencies.

In the case of radio astronomy, the signal-to-noise ratio is low. The signal coming from celestial sources is random just like thermal noise. Measuring the average power $\langle P \rangle$ of random signals requires lots of averaging. The fluctuation (intended as standard deviation) of the result ΔP only decreases with the square root of the number of measurements N according to the Dicke equation [9]:

$$\frac{\Delta P}{\langle P \rangle} = \frac{1}{\sqrt{N}} = \frac{1}{\sqrt{B \cdot \tau}} = \sqrt{\frac{B_{VIDEO}}{B}} = \frac{\Delta T}{\langle T \rangle}$$

In the case of a radio receiver, the number of independent measurements $N = B \cdot \tau$ is the product of the receiver bandwidth and measurement time. Most scanning-receiver type spectrum analyzers have built-in averaging in the form of a low-pass video filter with a cutoff frequency $B_{VIDEO} \ll B$ much smaller than their resolution bandwidth.

To observe the neutral-hydrogen radiation at $\lambda = 21\text{cm}$ a sensible setting is a resolution bandwidth of $B = 10\text{kHz}$. Setting the video bandwidth to $B_{VIDEO} = 10\text{Hz}$ is equivalent to an averaging factor of $N = 1000$. The fluctuation of the result is thus reduced by a factor of $\sqrt{1000} \approx 31.6$. The typical $\sim 10\text{dB}$ noise "grass" of a spectrum analyzer is reduced to $\sim 0.3\text{dB}$. Considering the noise sources in our radio telescope $T = T_{SKY} + T_s \approx 10\text{K} + 60\text{K} = 70\text{K}$, the standard deviation $\Delta T = \langle T \rangle / \sqrt{N} = 2.2\text{K}$ is a good estimate for the minimum observable signal coming from celestial sources.

Unfortunately such a measurement becomes very slow due to the inefficient use of the incoming signal energy by a scanning receiver. Observing the hydrogen frequency band of our Milky Way galaxy requires scanning a band of $\Delta f = 2\text{MHz}$. A single observation requires 20s although only 100ms are effectively used:

$$t = \frac{\tau \cdot \Delta f}{B} = \frac{\Delta f}{B_{VIDEO} \cdot B} = 20\text{s} \quad \tau = \frac{1}{B_{VIDEO}} = 100\text{ms}$$

On the other hand, if the same measurement is performed with a FFT spectrum analyzer, the latter making full use of the incoming signal energy, the observation time reduces to

$$t = \tau = 1/B_{VIDEO} = 100\text{ms}$$

Considering the rotation of the Earth and the beam width of the antenna used, a correction of the antenna direction is required about once per minute to track a selected deep-space radio source. A simple Python script "zvezdar.py" transforms the requested right ascension and

declination into azimuth and elevation including corrections for mechanical imperfections of the antenna rotor. EPR-203. Since its corresponding control unit EPS-103 only allows one command at a time, elevation and azimuth commands are sent by the Python script alternatively every 25 seconds through an RS-232 interface at 9600bps.

4.2. Sample measured spectra

A radio telescope for the neutral-hydrogen line does not see much radiation coming from dense, optically bright stars, but the radiation from sparse, lone hydrogen atoms. In the direction of the star Deneb (constellation Cygnus) three arms of our Milky Way galaxy can be seen due to their different Doppler shifts. Our Solar system is approaching all three arms (positive Doppler shift) at different relative velocities as shown on Figure 17:

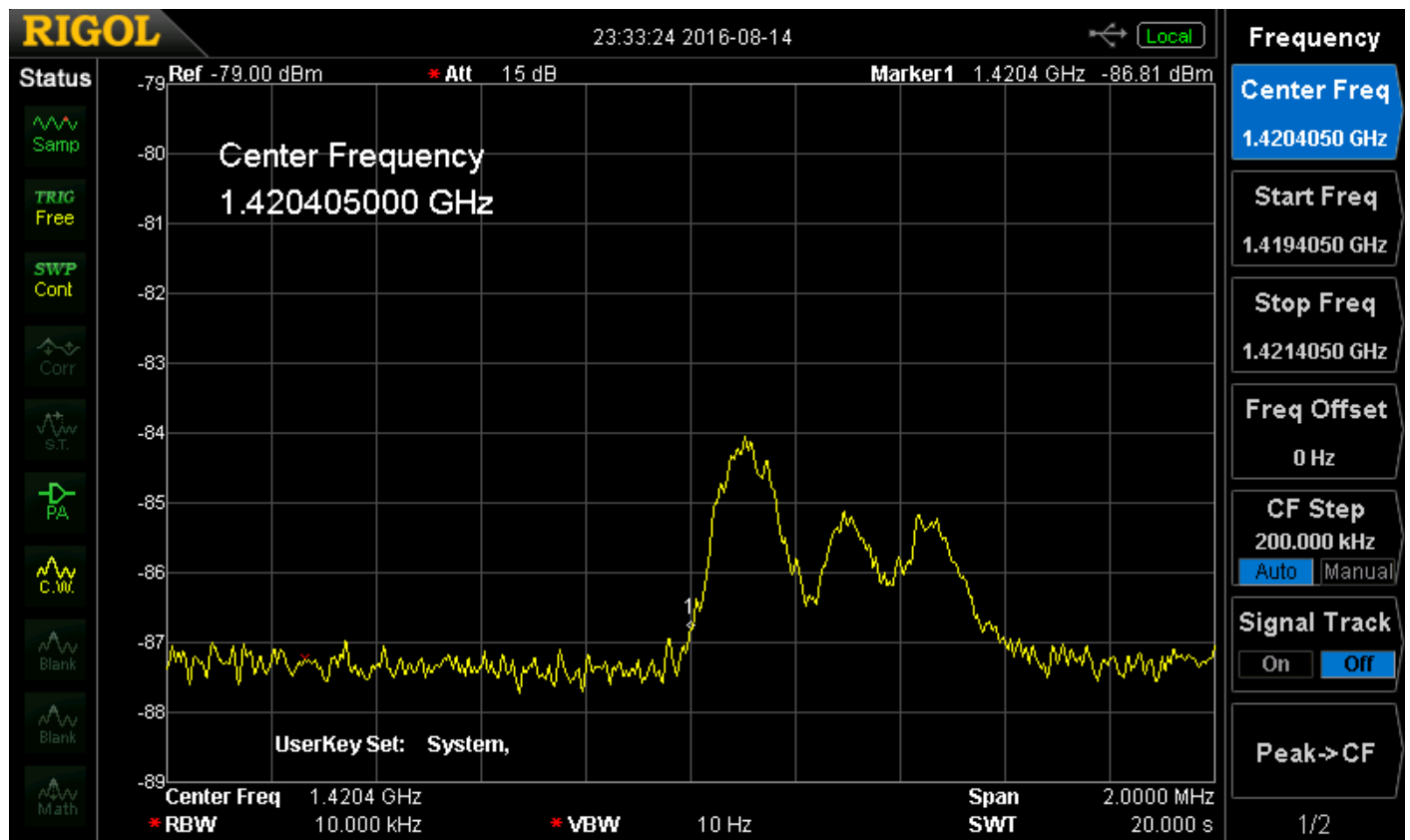


Figure 17: Neutral-hydrogen spectrum from the direction of the star Deneb.

On the other hand, the central part of our Milky Way galaxy is much denser resulting in a continuous neutral-hydrogen spectrum. Individual arms can hardly be resolved. The region in the direction of the constellation Scutum is moving away from our Solar system resulting in a negative Doppler shift as shown on Figure 18:



Figure 18: Neutral-hydrogen spectrum from the direction of the star α Scutum.

4.3. Measured hydrogen column density

Integrating the neutral-hydrogen power spectrum represented as the equivalent black-body brightness temperature $T(f)$, the total column density of neutral-hydrogen atoms can be derived:

$$\eta_H = \frac{8\pi \cdot k_B \cdot \tau_{1/2}}{h \cdot c_0 \cdot \lambda \cdot \ln 2} \cdot \int_{f_{MIN}}^{f_{MAX}} T(f) df$$

Inserting the physical constants in the above equation: the Boltzmann constant $k_B \approx 1.38 \cdot 10^{-23} \text{ J/K}$, the Planck constant $h \approx 6.63 \cdot 10^{-34} \text{ Js}$, the speed of light $c_0 \approx 3 \cdot 10^8 \text{ m/s}$, the excited neutral-hydrogen half life $\tau_{1/2} \approx 3.3 \cdot 10^{14} \text{ s}$ (~11 million years), the wavelength $\lambda = 21 \text{ cm}$ and referring the observed equivalent black-body brightness temperature $T(v)$ to the relative velocity in place of frequency $T(f)$, the above equation can be simplified into [10]:

$$\eta_H = 1.82 \cdot 10^{18} \cdot \frac{\text{atoms}}{\text{cm}^2} \cdot \int_{v_{MIN}}^{v_{MAX}} \frac{T(v)}{K} \cdot \frac{dv}{\text{km/s}}$$

Figure 18 shows the equivalent black-body brightness temperature $T(v)$ as a function of velocity calculated from the observed frequency spectrum in the direction of the star Deneb:

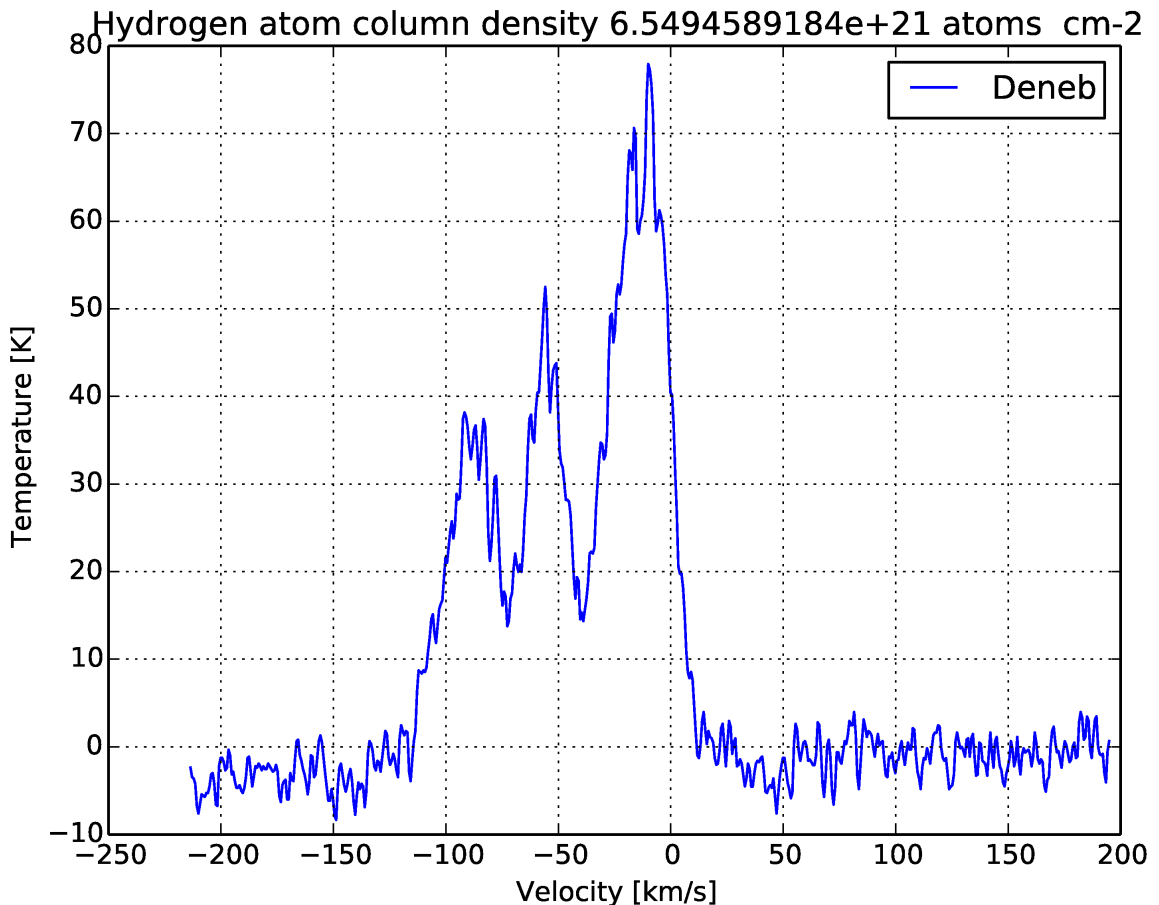


Figure 18: Neutral-hydrogen velocity and column density.

The integrated hydrogen-atom column density is about $\eta_H \approx 6.6 \cdot 10^{21} \text{ atoms/cm}^2$ spread over a distance of approximately $35000 \text{ light-years} \approx 3.3 \cdot 10^{20} \text{ m} = 3.3 \cdot 10^{22} \text{ cm}$. The average hydrogen density in the interstellar space is therefore very low, just $N_H \approx 0.2 \text{ atoms/cm}^3 = 2 \cdot 10^5 \text{ atoms/m}^3$ or very good vacuum indeed...

5. Hydrogen mapping of our galaxy

5.1. Software signal processing

Radio astronomy and in particular interferometry were one of the first large-scale applications of digital-signal processing. The reason is very simple: the signal-to-noise ratio in radio astronomy is always low. Therefore just a few bits of resolution are required to adequately represent and process the signals, simplifying the hardware. For example, interferometry works with just one-bit signal sampling and quantization.

Rather than using exotic hardware in the described radio telescope, an inexpensive DVB-T USB dongle based on the RTL2832U chip was used for frequency down conversion and A/D conversion. Besides a dedicated DVB-T demodulator, the RTL2832U chip includes a straightforward 8-bit A/D converter for analog radio reception. The latter is well supported both with drivers, application software and development tools in all known operating systems on personal computers. The A/D converter can process signal bandwidths up to $B \approx 2.4 \text{ MHz}$. The latter is more than sufficient to observe the neutral-hydrogen spectrum of our Milky Way galaxy.

The RTL2832U chip is frequently coupled with the R820T2 tuner (down converter) chip. Although the latter is only specified up to $f_{MAX} \geq 1 \text{ GHz}$, most chips exceed $f_{MAX} \geq 1.7 \text{ GHz}$ at room temperature. The R820T2+RTL2832U combination therefore allows direct processing of the

amplified and filtered 1.42GHz hydrogen-line signal provided that the tuner chip R820T2 is kept at a constant room temperature. An improved version of the DVB-T dongle is used in our radio telescope featuring a TCXO frequency reference in an aluminum case. The latter provides both shielding and cooling of all internal components as shown on Figure 19:



Figure 19: Inexpensive SDR front-end.

Although excellent open-source development tools exist for the R820T2+RTL2832U combination, ready-made software was tried first with excellent results. In particular we successfully experimented the freeware "HDSDR version 2.76" [11] running on "WindowsXP". The DVB-T dongle requires its own low-level USB driver "zadig_xp.exe" and the corresponding interface "ExtIO_RTL2832.dll" to HDSDR. The main advantage of HDSDR over other similar software is the ability to use large averaging factors and display small amplitude differences, both of them very necessary for radio astronomy.

We only used the radio-frequency FFT spectrum analyzer included besides several other receiver functions in HDSDR. A center frequency of $f_0 = 1420.405\text{MHz}$ and an observation span of $\Delta f = 1.44\text{MHz}$ are good choices for hydrogen-line observations of our Milky way galaxy. The optimum FFT size was found experimentally as $2^{14} = 16384$ to separate easily hydrogen spectra from narrow-band interference.

The spectrum is first averaged by a factor of 2048 inside HDSDR. The averaged spectrum is displayed on a 1280-pixel wide LCD screen, therefore 16384 spectrum lines are further averaged by a factor of about 13 to 1280 display columns. All this averaging reduces the power (temperature) fluctuations to approximately $10\text{dB}/\sqrt{2048 \cdot 13} \approx 0.06\text{dB}$.

The "HDSDR" software can display the averaged spectrum plot as a function of frequency or as a spectrum waterfall with different colors indicating signal intensity. Further, the waterfall can be made slow enough to allow mechanical scanning of the sky and its color scale can be selected to show intensity changes of less than 0.5dB. One of the first experiments with "HDSDR" running independently on two personal computers showing 2D images (galactic longitude and relative velocity) of our Milky Way galaxy is shown on Figure 20:

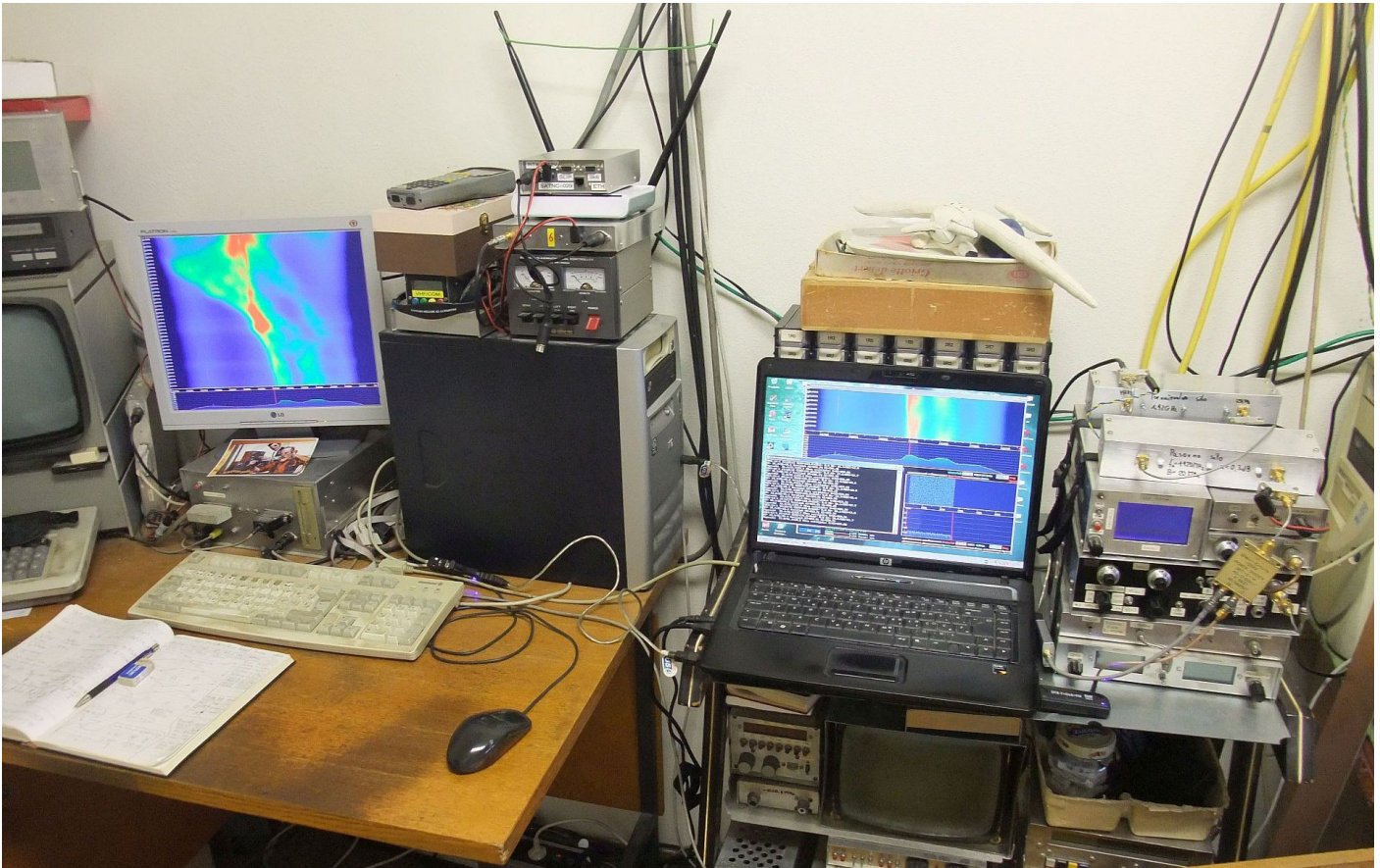


Figure 20: Waterfall display with HDSDR software.

The A/D converter inside the RTL2832U chip includes an analog anti-aliasing filter on its input. The latter has a ripple of about +/-0.5dB over the central three quarters of the observed frequency span and rolls off sharply (about -3dB) at both span edges. This is an excellent result for an analog filter and in most applications goes unnoticed. On the other hand, radio astronomy requires measuring very small differences of signal levels. Unfortunately the current version of the HDSDR freeware does not include a normalization of the response nor other countermeasures to correct the above-mentioned pass-band ripple.

5.2. Galactic-plane scanning

One of the most important historical discoveries of hydrogen-line observations is that our Milky Way is a spiral galaxy. The plane of the Milky Way is currently inclined by 62.8° with respect to the equatorial plane. This inclination is slowly increasing due to the precession of the Earth's rotation axis. Most of the hydrogen-line radiation comes from the plane of our galaxy. Hydrogen-line radiation from other directions is much weaker since its sources are much farther away. Therefore the plane of the Milky Way is the target of choice to begin with hydrogen-line observations.

The whole galactic plane is currently not visible from our latitude 46° north. Considering the beam width of a 3.1m-diameter antenna at 1.42GHz, celestial objects can only be observed at elevations larger than $EL \geq 10^\circ$ above the local horizon to avoid thermal noise radiated by the warm ground. In our case we were lucky enough not to have any obstacles nor interference sources in the direction south where the most difficult-to-see celestial objects appear at particular times during the day.

Galactic coordinates, galactic longitude and galactic latitude, are the coordinates of choice for hydrogen-line observations. The galactic plane of our Milky Way galaxy is by definition galactic latitude zero $GLAT=0$. Galactic longitude zero $GLON=0$ is defined by radio observations as

the powerful radio source Sagittarius A, supposed to be a very massive black hole in the center of our galaxy. Galactic longitude increases in the opposite direction of the rotation of our galaxy. The angular velocities of different parts of our galaxy are different resulting in Doppler shifts.

Our scanning of the galactic plane is explained using the artist's impression of the Milky Way [12]. Sagittarius A has a declination of about $\delta \approx -29^\circ$, therefore it reaches a elevation of just 15° above the southern horizon at our latitude 46° north. It therefore makes sense to start the galactic-plane scanning just before Sagittarius A at a galactic longitude of about $GLON = -10^\circ$. The observed galactic longitude is then increased at a carefully selected rate for about 12 hours to end our scanning around galactic longitude $GLON = 265^\circ$ as shown on Figure 20:

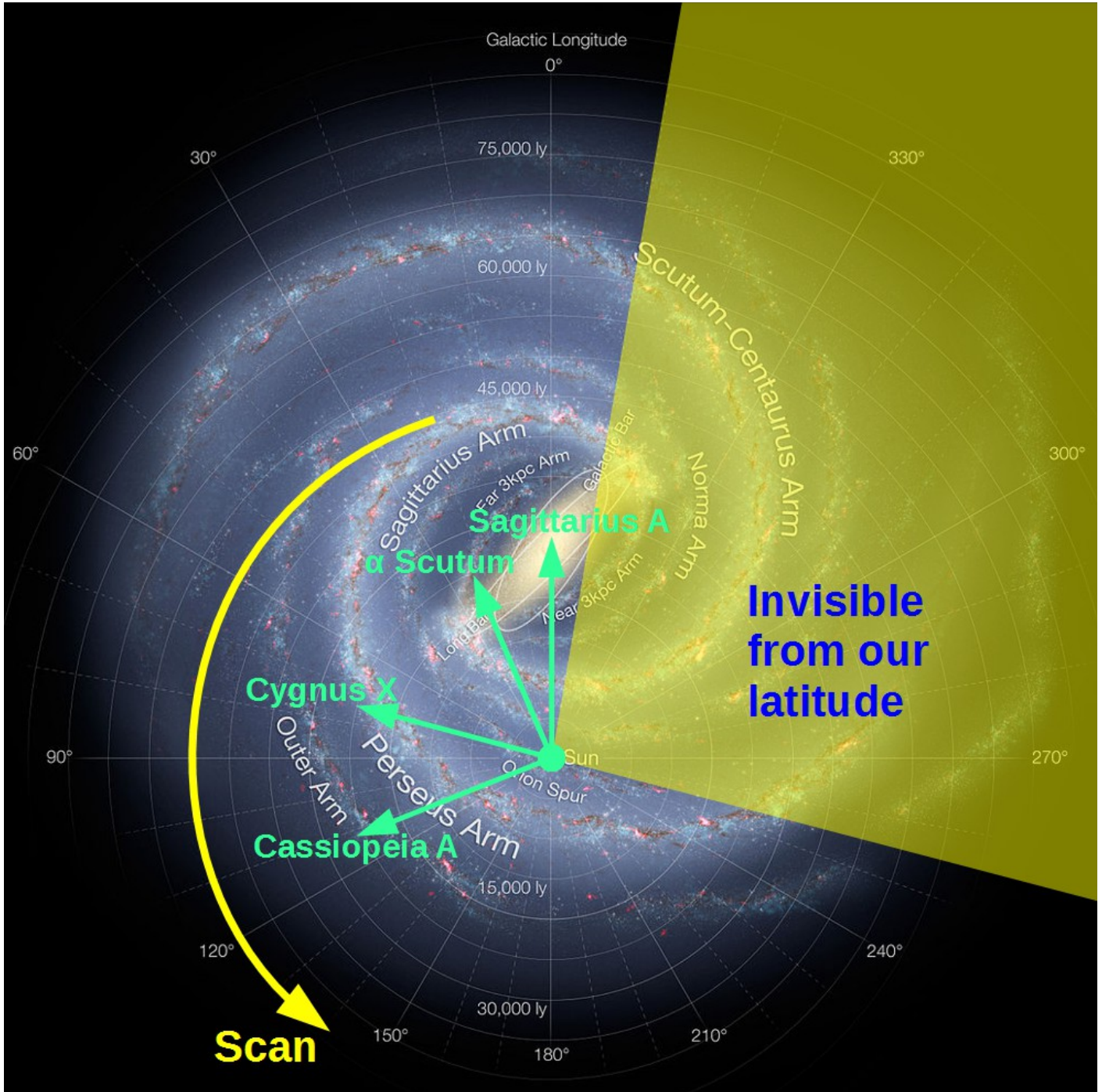


Figure 20: Galactic-plane scanning from our latitude.

In this way the whole visible galactic arc is observed during one single scan with plenty of time for data averaging. Considering the rotation of the Earth such a scan both starts and ends at the southern horizon. The direction of the scan is important. Scanning by increasing the galactic longitude the galactic equator appears high above the local horizon at our latitude 46° north. On the other hand, scanning in the opposite direction, decreasing the galactic longitude from $GLON = 265^\circ$ to $GLON = -10^\circ$, the galactic equator appears rather low above our northern

horizon. Unfortunately local obstructions at our micro location preclude such scanning.

Besides steering the antenna positioner to scan the galactic plane, the Python script "mlekar.py" also records the times and corresponding galactic longitudes and latitudes in a text file. On the other hand, the "HDSDR" software puts time tags on the waterfall display. By combining both, the waterfall can be referenced to the galactic longitude. Since the computer screen is not high enough, periodic screen-shots are taken with the "Chronolapse" software and the final result is stitched together with the "IrfanView" image-processing software as shown on Figure 21:

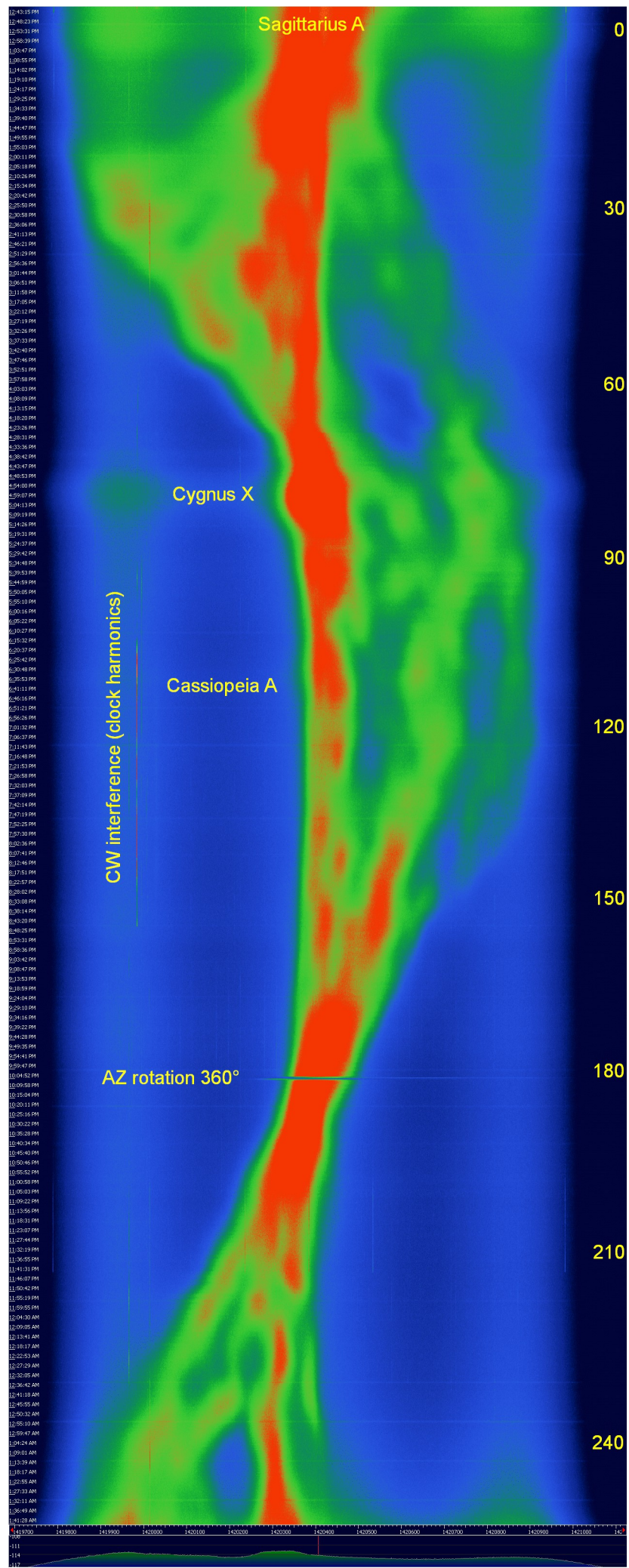


Figure 21: Waterfall display with HDSDR software.

Figure 21 shows unprocessed and uncorrected data. Besides the hydrogen spectrum, continuum (broadband) celestial sources are also visible like the center of our galaxy, the star-forming region Cygnus X or the supernova remnant Cassiopeia A. Ground thermal noise is visible at the beginning and at the end of the scan including the ripple of the analog anti-aliasing filter in our receiver. Narrow-band CW interference (clock harmonics from digital equipment) is visible as narrow spectral lines around 1420.000MHz. Periodic wide-band interference (likely spark ignition) is visible towards the end of the scan. The interruption at galactic longitude 180° is due to our programming mistake of the rotor control unit EPS-103 causing a 360° rotation of our antenna.

5.3. 3D map of the Milky way

Performing several galactic-longitude scans at different galactic latitudes, a 3D map of our galaxy can be built. Considering the beam width of our antenna, separate scans were made in 5° galactic-latitude steps. A map composed of five such scans at galactic latitudes of -10°, -5°, 0°, +5° and +10° is shown on Figure 22:

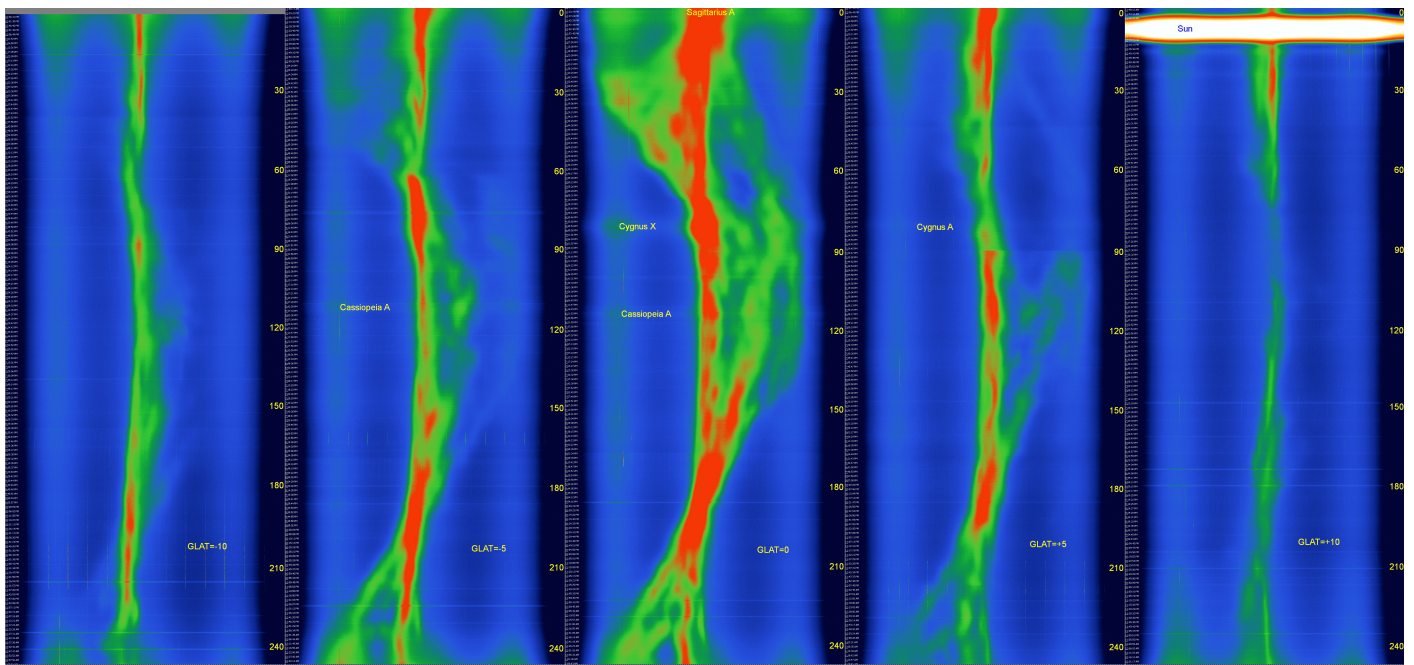


Figure 22: Measured 3D map of the Milky Way.

Observing southern galactic latitudes becomes increasingly more difficult from the northern hemisphere. Missing data at galactic latitude -10° (south) had to be replaced with a gray bar at the beginning of the scan. On the other hand, the time of year of the galactic-longitude scan at galactic latitude +10° (north) was intentionally selected to cross the Sun.

The most interesting scan is in the galactic plane (galactic latitude 0°) showing even distant arms of our galaxy with large Doppler shifts of the hydrogen line. Moving away from the galactic plane either south or north the amount of visible hydrogen decreases. Even more important, moving away from the galactic plane only local hydrogen with a relatively small Doppler shift remains visible.

6. Conclusion

In order to understand the difficulties in operating a radio telescope, it is fair to compare its performance a well-known device like a GSM phone operating in the nearby 1.8GHz frequency band. Both the hydrogen line of a single galactic arm and the GSM signal have a similar bandwidth of about $B \approx 200\text{kHz}$. While the GSM phone requires a signal with the equivalent black-body

brightness temperature of $T_{GSM} \approx 30000\text{K}$, the arms of our galaxy on average reach $T_{GALAXY} \approx 30\text{K}$. GSM signals are therefore stronger by a factor of $1000 = 30\text{dB}$ than hydrogen-line signals.

The presented compact radio telescope has an antenna with an effective area about $10000 = 40\text{dB}$ times larger than a GSM phone. Large professional radio telescopes have effective areas about $1000 = 30\text{dB}$ times larger than our radio telescope. In total, our compact radio telescope is about 70dB more sensitive than a GSM phone and about 30dB less sensitive than a large professional radio telescope.

Nevertheless we were able to obtain a 3D map, intensity versus galactic longitude, galactic latitude and Doppler shift of our Milky Way galaxy with our compact radio telescope. Such a 3D map lead to the discovery of the spiral structure of our galaxy some 60 years ago using much larger instruments. A further limitation of our compact radio telescope is its location at 46° northern latitude while the most interesting features of our galaxy and neighbor celestial objects are located in the southern sky.

Our results were obtained using signal-processing software that was not originally designed for radio-astronomical observations. Much improvement could be obtained by writing or own code to allow response normalization, arbitrary averaging factors and known radio-interference rejection. In this was the hydrogen spectra of less bright celestial objects could be observed like the Andromeda galaxy as well as many continuum sources like some of the strongest pulsars. Of course, the most ambitious goal are radio interferometers with arbitrary baselines including several similar compact radio telescopes, synchronized using GNSS (global satellite navigation systems) and linked via internet.

7. References

- [1] Grote Reber: "Galactic Radio Waves", Sky and Telescope, Vol.8, No.6, April, 1949.
- [2] Mal Wilkinson, John Kennwell: "Hydrogen-line observations of the Galaxy and the Magellanic Clouds", Australian Journal of Astronomy, Vol.5, No.4, pp 121-133, 1994.
- [3] Jean-Jacques Maintoux: "Radioastronomie",
http://f1ehn.pagesperso-orange.fr/fr/f_radioastro.htm
- [4] Nguyen Van Hiep, Pham Tuan Anh, Pham Ngoc Diep, Pham Ngoc Dong, Do Thi Hoai, Pham Thi Tuyet Nhung, Nguyen Thi Thao, Pierre Darriulat: "The VATLY Radio Telescope", Communications in Physics, Vol.22, No.4, pp 365-374, 2012.
- [5] A. Kumar, "Reduce Cross-Polarization in Reflector-Type Antennas," Microwaves, pp 48-51, March 1978.
- [6] B.W. Malowanchuk, VE4MA, "Use of Small TVRO Dishes for EME," Proceedings of the 21st Conference of the Central States VHF Society, ARRL, pp 68-77, 1987.
- [7] Matjaž Vidmar: "Ein sehr rauscharmer Antennenverstarker fuer das L-band", pp 163-169, UKW Berichte, 3/1991, or "A Very Low Noise Aerial Amplifier", pp 90-96, VHF Communications, 1992/2.
- [8] Solar Radio Data, U.S. Dept. of Commerce, NOAA, Space Weather Prediction Center,
http://legacy-www.swpc.noaa.gov/ftpdir/lists/radio/7day_rad.txt
- [9] Robert H. Dicke: "The Measurement of Thermal Radiation at Microwave Frequencies.", The Review of Scientific Instruments, Vol.17, No.7, pp 268-275, 1946.
- [10] James J. Condon, Scott M. Ransom, NRAO: "The HI 21 cm Line",

<http://www.cv.nrao.edu/course/astr534/HILine.html>

[11] High Definition Software Defined Radio, <http://www.hdsdr.de/>

[12] Artist's impression of the Milky Way (updated - annotated),
[https://commons.wikimedia.org/wiki/File:Artist's_impression_of_the_Milky_Way_\(updated_-_annotated\).jpg](https://commons.wikimedia.org/wiki/File:Artist's_impression_of_the_Milky_Way_(updated_-_annotated).jpg)

* * * * *